AD-A176 777 BLUE-GREEN LASER DIODE RESEARCH PROGRAM(U) MINNESOTA MINING AND MFG CO ST PAUL ELECTRONIC AND INFORMATION SECTOR LAB T L SMITH ET AL. JAN 87 N00014-85-C-0552 1/1

UNCLASSIFIED F/G 20/5 NL

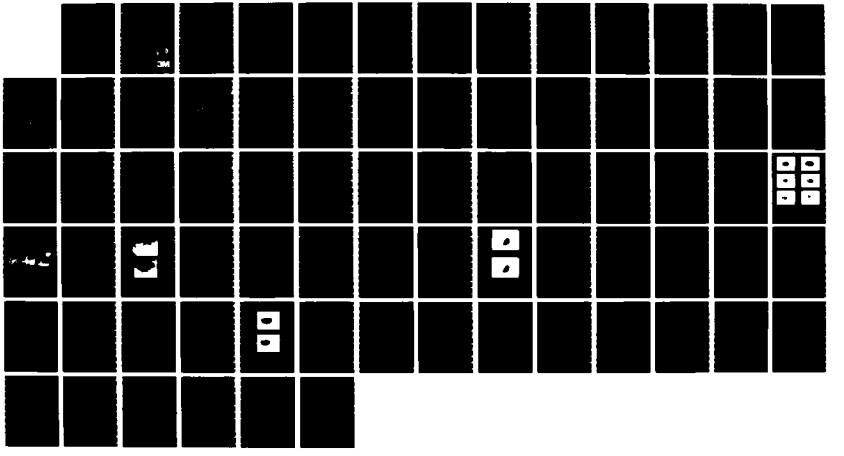

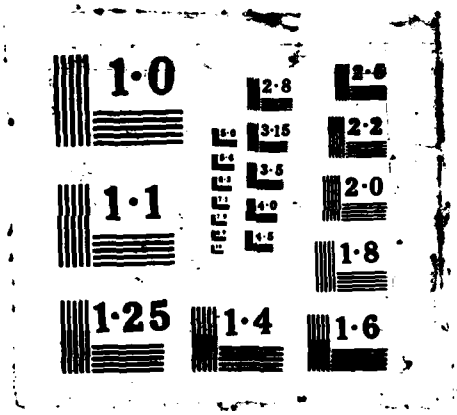
1·0
1·1
1·25
1·4
1·6
1·8
2·0
2·2
2·8
3·15

(12)

BLUE-GREEN LASER DIODE RESEARCH PROGRAM

Quarterly Technical Progress Report No. 3
For The Period October 1, 1986 To December 31, 1986

Prepared Under
Contract Number N00014-85-C-0552

JANUARY, 1987

Work supported in part by the:

DEFENSE ADVANCED RESEARCH PROJECTS AGENCY
1400 Wilson Boulevard
Arlington, VA 22209

Under the:

OFFICE OF NAVAL RESEARCH
Department Of The Navy
800 N. Quincy Street
Arlington, VA 22217-5000

Electronic and Information
Sector Laboratories/3M
St. Paul, MN 55144

3M

REPORT DOCUMENTATION PAGE

1a. REPORT SECURITY CLASSIFICATION UNCLASSIFIED	1b. RESTRICTIVE MARKINGS
2a. SECURITY CLASSIFICATION AUTHORITY	3. DISTRIBUTION/AVAILABILITY OF REPORT Approved For Public Release Distribution Unlimited
2b. DECLASSIFICATION/DOWNGRADING SCHEDULE	
4. PERFORMING ORGANIZATION REPORT NUMBER(S) Quarterly Technical Progress Report No. 3	5. MONITORING ORGANIZATION REPORT NUMBER(S)
6a. NAME OF PERFORMING ORGANIZATION 3M Company 6b. OFFICE SYMBOL (If applicable)	7a. NAME OF MONITORING ORGANIZATION Defense Advanced Research Projects Agency
6c. ADDRESS (City, State and ZIP Code) E&IT Sector Laboratory - 201-1N-36 3M Center - St. Paul, MN 55144	7b. ADDRESS (City, State and ZIP Code) 1400 Wilson Boulevard Arlington, VA 22209
8a. NAME OF FUNDING/SPONSORING ORGANIZATION Office of Naval Research 8b. OFFICE SYMBOL (If applicable)	9. PROCUREMENT INSTRUMENT IDENTIFICATION NUMBER Contract No. N00014-85-C-0552
8c. ADDRESS (City, State and ZIP Code) Dept. of the Navy 800 N. Quincy St. Arlington, VA 22217-5000	10. SOURCE OF FUNDING NOS. PROGRAM ELEMENT NO. / PROJECT NO. / TASK NO. / WORK UNIT NO.
11. TITLE (Include Security Classification) Blue-Green Laser Diode Research Program	
12. PERSONAL AUTHOR(S) Drs. T.L. Smith and C.T. Walker	
13a. TYPE OF REPORT Technical Progress 13b. TIME COVERED FROM 86/10/1 TO 86/12/31	14. DATE OF REPORT (Yr., Mo., Day) 1987, January 15. PAGE COUNT 72
16. SUPPLEMENTARY NOTATION	

17. COSATI CODES			18. SUBJECT TERMS (Continue on reverse if necessary and identify by block number)
FIELD	GROUP	SUB. GR.	Blue-Green Laser or Lasers, Blue-Green

19. ABSTRACT (Continue on reverse if necessary and identify by block number)

During this reporting period, efforts were begun to incorporate Na and N acceptors in ZnSe. Other efforts underway included studies of the effects of growth rate on unintentionally-doped ZnSe, studies of the effectiveness of present substrate preparation procedures, studies of gain and dynamics in electron-beam-pumped lasing, Schottky and ohmic contact work, growth of ZnSe on Si using ZnSe/Ge superlattice buffer layers, and x-ray double crystal rocking curve comparative studies of the structure of ZnSe/GaAs and ZnSe/Ge. Significant progress was made in all of the above areas.

20. DISTRIBUTION/AVAILABILITY OF ABSTRACT UNCLASSIFIED/UNLIMITED ☐ SAME AS RPT. ☒ DTIC USERS ☐	21. ABSTRACT SECURITY CLASSIFICATION UNCLASSIFIED
22a. NAME OF RESPONSIBLE INDIVIDUAL L.C. McGraw	22b TELEPHONE NUMBER (Include Area Code) (612) 733-9816 22c. OFFICE SYMBOL

DD FORM 1473, 83 APR EDITION OF 1 JAN 73 IS OBSOLETE.

EXECUTIVE SUMMARY

In the first quarter of the second program year, both the St. Paul and Toronto groups began efforts to incorporate acceptors in ZnSe. The St. Paul group concentrated on Na, while the Toronto group concentrated on N. Other efforts underway in St. Paul included studies of the effects of growth rate on unintentionally-doped ZnSe, studies of the effectiveness of present substrate preparation procedures, studies of gain and dynamics in electron-beam-pumped lasing, and Schottky and ohmic contact work. Other efforts underway in Toronto included the growth of ZnSe on Si using ZnSe/Ge superlattice buffer layers, and x-ray double crystal rocking curve comparative studies of the structure of ZnSe/GaAs and ZnSe/Ge. Significant progress was made in all of the above areas.

In the Na-doping work, it was found that the incorporation of Na from the Na_2Se source was strongly dependent upon the ZnSe growth conditions. Under appropriate conditions, Na doping concentrations exceeded 2×10^{17} cm^{-3}. The presence of Na acceptor levels was reflected in donor-acceptor pair photoluminescence, but only weak indications of acceptor bound exciton emission were seen. In all cases, the PL spectra continued to be dominated by the I_x donor-bound excitonic emission, and in fact, the width of the I_x peak increased with Na_2Se temperature, suggesting increasing contamination with the donor responsible for I_x. This observation was consistent with electrical measurements which showed increasing electron concentration with increasing Na_2Se oven temperature. Because of the fact that the donor concentration increases before significant incorporation of Na begins, it is possible that the Na_2Se source material is contaminated, probably with Cl. It is also possible that the presence of the Na_2Se flux somehow results in effective growth conditions which deviate from those desired; this is supported by the observation of abnormal RHEED patterns during Na_2Se doping. Efforts to check these possibilities are underway. Meanwhile, attention will be turned to P doping using Zn_3P_2 (which can be obtained in higher purity than the Na_2Se), and possibly Na doping using a metal source.

The results achieved using gaseous N_2 for doping are currently more promising. Although SIMS measurements of the N incorporation have not yet been performed, the presence of N acceptor levels is confirmed by the observation of dominant acceptor-bound and strong donor-acceptor pair photoluminescence. Additionally, RHEED studies indicate no disruption of surface morphology, even at the high N_2 pressures (10^{-4} mbar) used during growth. Nevertheless, electrical characterization indicates that the N-doped samples are of high resistivity and still n-type. At present the effects of growth parameters on the N acceptors are being studied; soon attempts will be made to perform doping with an ionized nitrogen beam.

In additional work on unintentionally doped ZnSe, repetition of earlier growth rate studies has indicated no significant dependence of film quality on growth rate for growth rates between 0.5 and 1.0 μ/hr. This result is in conflict with results reported last quarter; the earlier results are believed to be in error due to problems in substrate temperature control.

In-situ Auger spectroscopy studies of surface contamination on GaAs wafers used in the two-chamber St. Paul MBE system have indicated that recontamination of the substrates with O and C occurs during transport of the substrate from III-V chamber (where desorption is performed) to the II-VI growth chamber. This problem is being solved by addition of a short, lower temperature desorption step in the II-VI chamber.

Several ZnSe films have been grown on Si wafers with 2 and 10 period superlattice buffer layers. Although the 2 period superlattice produces a marked improvement in film quality (as judged by PL), the 10 period buffer does not. This observation is not understood at present.

X-ray double crystal rocking curve (DCRC) studies of ZnSe/GaAs and ZnSe/Ge have revealed that the observed DCRC linewidth is a strong function of the angular position of the sample, and that the epitaxial film crystal axes are misoriented with respect to the substrate. This means that the linewidth must be recorded at several sample rotation angles in order to avoid erroneous conclusions.

Measurement of gain and lasing dynamics in electron-beam pumped ZnSe are continuing. Comparison of cathodoluminescence efficiencies for our MBE-grown material to those for OMVPE material (obtained from B. Wessels at Northwestern University) indicate that the MBE material is at least 10 times as efficient.

Problems are still being experienced in making high-quality, reproducible ohmic and Schottky contacts to ZnSe. It is hoped that the implementation of the in-situ metallization facility, scheduled for the second quarter of this program year, will solve these problems.

TABLE OF CONTENTS

LIST OF FIGURES

LIST OF FIGURES (continued)

LIST OF TABLES

1.0 INTRODUCTION

This report covers progress during the thirteenth through fifteenth months of ONR Contract N00014-85-C-0552. The various sections of the report are numbered and titled using the format of the original proposal. As before, results from parallel programs at 3M-St. Paul and 3M-Toronto are discusssed.

2.0 PROGRESS REPORT

2.1 Project 1, Task 1: Materials Research - Undoped ZnSe Research

This quarter, both the St. Paul and Toronto groups continued to expend some effort in growth of unintentionally-doped ZnSe. The St. Paul group investigated the effects of film growth rate on film properties, and the effects of the substrate preparation procedure on the residual surface contamination of the GaAs substrates. Additionally, selective excitation photoluminescence (SEPL), Raman scattering, capacitance spectroscopy, and SIMS evaluations of unintentionally-doped material continued. In Toronto, a comparative study of the structure of ZnSe/GaAs and ZnSe/Ge using double-crystal x-ray diffractometry was completed. Also, a study was made of ZnSe films grown on Si with ZnSe-Ge superlattice buffer layers.

2.1.1 Unintentionally-Doped ZnSe Heteroepitaxy on (100) GaAs

2.1.1.1 The Growth of Unintentionally-Doped ZnSe On (100) GaAs

During the past three months, seven unintentionally-doped ZnSe on (100) GaAs samples were grown in St. Paul. In the first few runs, a reproducibility problem was discovered. Films grown under growth conditions identical to those used in the past showed the different PL spectra. Careful examination of the growth parameters indicated that the growth temperatures were actually well above the desired ones, and that this caused deterioration of the film quality. It is believed that the false temperature reading is due to a malfunction in the thermocouple circuit inside the vacuum system. Currently we are using an infrared pyrometer to monitor the substrate temperature. This pyrometer is calibrated against the desorption temperature of oxide from GaAs (~ 580°C).

After the substrate temperature problem had been resolved, two layers (ZSE66 and ZSE67) were grown at the same substrate temperature (350°C) and same beam pressure ratio (1/2:1). However, the absolute beam pressures of both Zn and Se for the former sample are only half of those for the latter. In order to achieve the same film thickness to facilitate comparison, the growth time of ZSE66 was twice that of the growth time for ZSE67. During the growth, the RHEED patterns were the same for both specimens and their

growth rates were 0.5 and 0.9 μm/hour, respectively. Results of Hall and low temperature photoluminescence measurements indicated that the film quality does not deteriorate as the growth rate increases from 0.5 to 1.0 μm/hour. (See sections 2.1.1.2 and 2.1.1.4.) Note that this result disagrees with the preliminary study reported earlier. We attribute this discrepancy to the earlier problems of substrate temperature control.

Late in this quarter, a Scanning Auger Microprobe (SAM) was installed in a separate UHV chamber gated to the UHV transfer tube. This makes it possible to study the surface cleanliness of the GaAs substrate prior to epitaxial growth, without exposing the substrate to air. With this new capability, we have recently studied the effectiveness of our substrate preparation procedure and refined our growth procedure; these refinements may further improve the quality of our ZnSe films.

Figure 2-1 (a) shows the Auger Spectrum of an as-loaded GaAs substrate which has been degreased and etched. The main species detected on the surface are Ga, As, and O; a trace amount of carbon was also detected.

The amount of C present is comparable to that observed by other workers [1], therefore we believe that our substrate cleaning procedure is reasonably good.

Figure 2-1 (b) shows the spectrum of a GaAs substrate after desorption in the III-V chamber and transfer through the pipeline to the Auger Chamber. This transfer step is similar to the one in an actual growth run (from III-V chamber to II-VI chamber). Therefore, it is important to know whether contamination may occur during the transfer. As shown in the spectrum, carbon and oxygen are still present on the surface.

However, from the above observations, it cannot be ascertained whether the contamination observed at this point is due to incomplete desorption or due to recontamination during the transfer step. Figure 2-1 (c) shows the spectrum of a desorbed GaAs substrate which has been subjected to the transfer step and then re-desorbed briefly at 500°C. The removal of both O and C is now nearly complete. In the future, a brief re-desorption at 500°C will be carried out in the II-VI chamber immediately before growth of the ZnSe film, and effects on film quality will be studied.

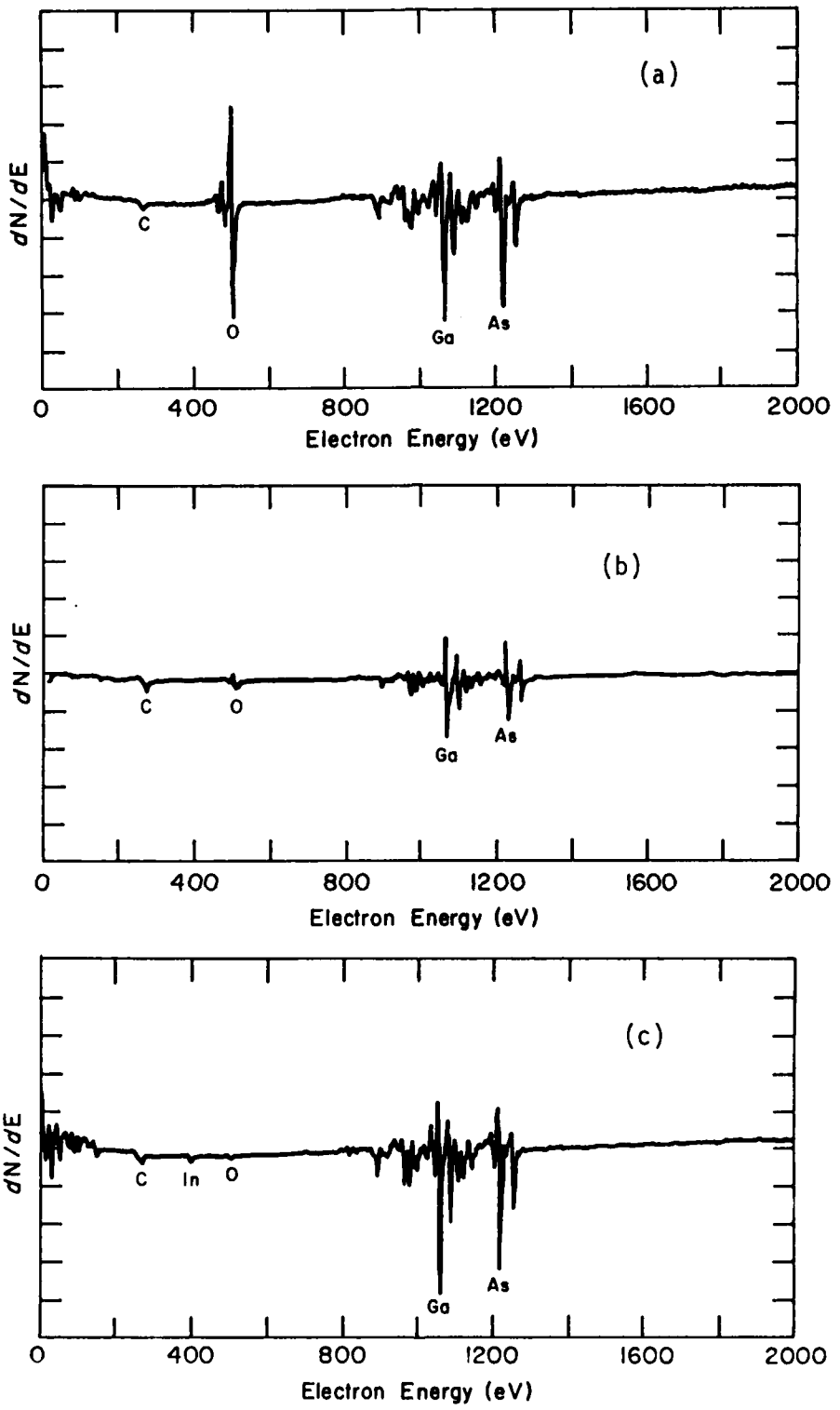

Figure 2-1. Auger spectra of GaAs substrates during various stages of thermal desorption.
(a) spectrum of as-loaded wafer
(b) spectrum of wafer after desorption in III-V chamber and transfer to Auger chamber, and
(c) spectrum after second flash desorption to 500°C in Auger chamber.

2.1.1.2 Photoluminescence of Unintentionally-Doped ZnSe on (100) GaAs

Photoluminescence (PL) measurements on samples in the growth matrix study were completed and correlated with electrical measurements on these same samples. We have identified certain properties of the PL spectra which serve as indicators of film quality and which vary systematically with variations in growth conditions. Figures 2-2 and 2-3 show that the intensity of the dominant neutral-donor-bound exciton (DBE), I_x, and the ratio, R, of the peak near-band-edge (NBE) emission to the deep level (DL) emission, both exhibit maxima near the growth conditions which we feel are optimum--T_g = 300 - 350°C, BPR = 1.0 - 2.0. Figure 2-4 demonstrates that reasonable correlations exist between the intensity of I_x and the room-temperature electron concentration [Figure 2-4 (a)], between the low-temperature R-value and the peak mobility [Figure 2-4 (b)], and between the linewidth of I_x and the low-temperature mobility [Figure 2-4 (c)]. The correlation between I_x and n_{300} indicates that the PL DBE line is related to that donor which is providing the electrically-active carriers. Since the R-value is degraded by the presence of deep scattering centers and traps, it should correlate with the peak mobility, as observed. Finally, the PL peak linewidths are increased by the presence of the same ionized defects which limit the low-temperature mobility.

In the course of analyzing these PL measurements, it has been necessary to develop routines to deconvolute spectra resulting from two or more closely-spaced peaks. This has been accomplished using a commercial software package ('ASYST', McMillan Software Co.) The routine accepts, as starting values, estimates of the intensities, widths, and energies for two to four peaks. It then calculates the resultant intensity for the sum of Lorentzian peaks, compares to the measured intensity profile, and adjusts the peak parameters until the differences are minimized. An example of the result of this fitting procedure, applied to one of the samples (ZSE53A) from the growth matrix study, is shown in Figure 2-5.

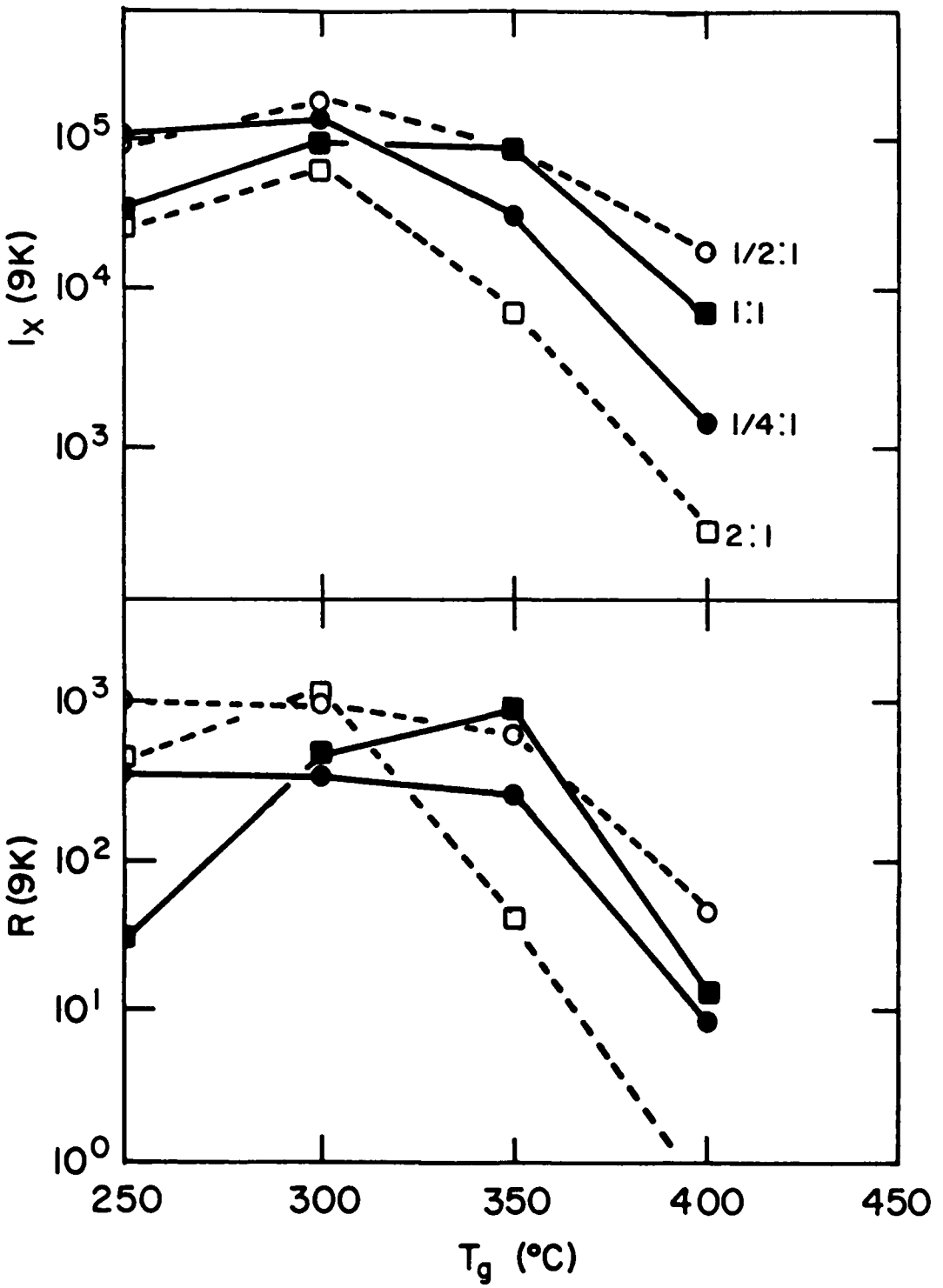

Figure 2-2. Top: Variations in the intensity of the dominant 9K near-band-edge emission peak, I_x, for different substrate temperatures.
Bottom: Variations in the 9K R-value (NBE intensity/DL intensity) for different substrate temperatures.

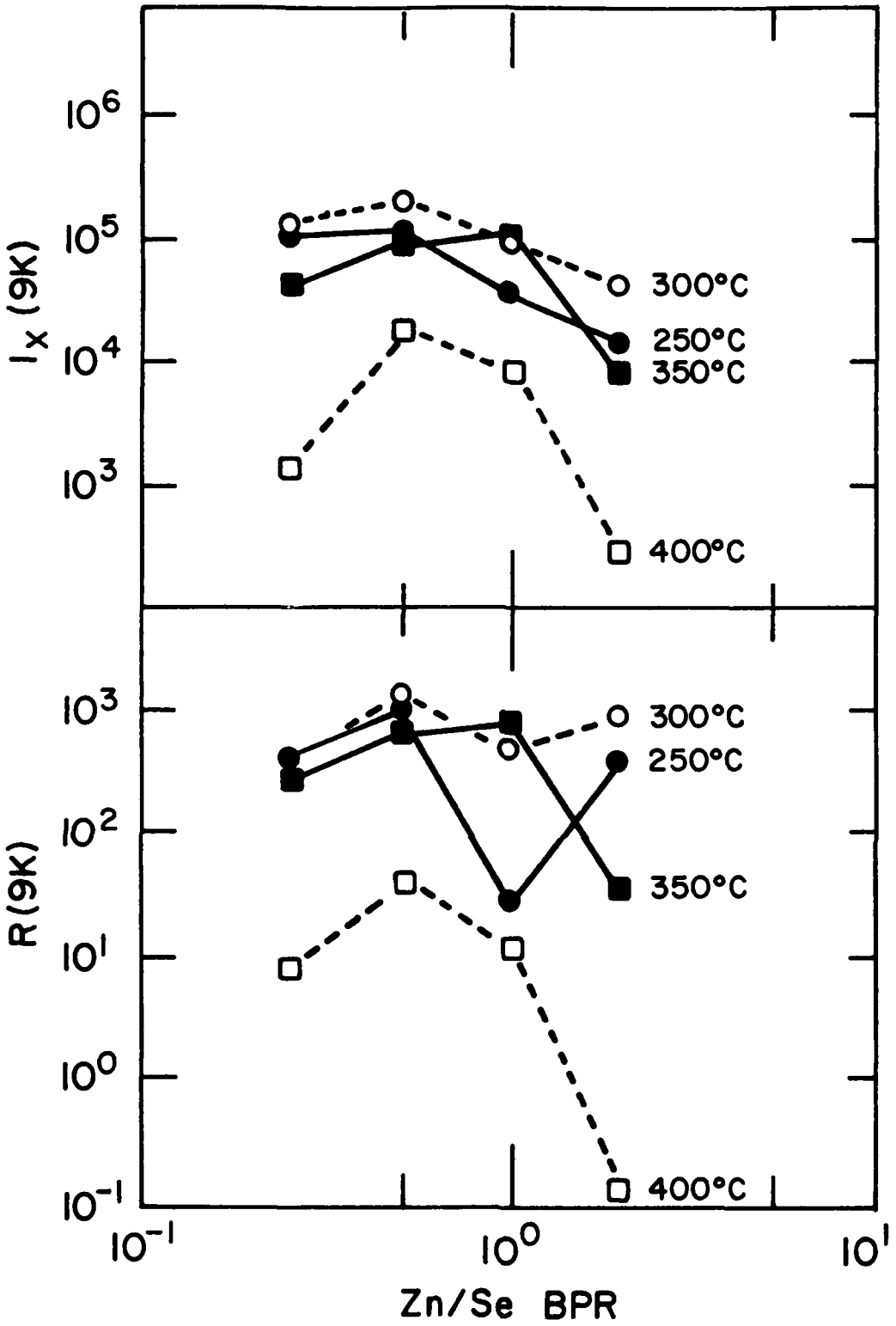

Figure 2-3. Top: Variations in the intensity of the dominant 9K near-band-edge emission peak, I_x, for different Zn/Se beam pressure ratios.
Bottom: Variations in the 9K R-value (NBE intensity/DL intensity) for different Zn/Se beam pressure ratios.

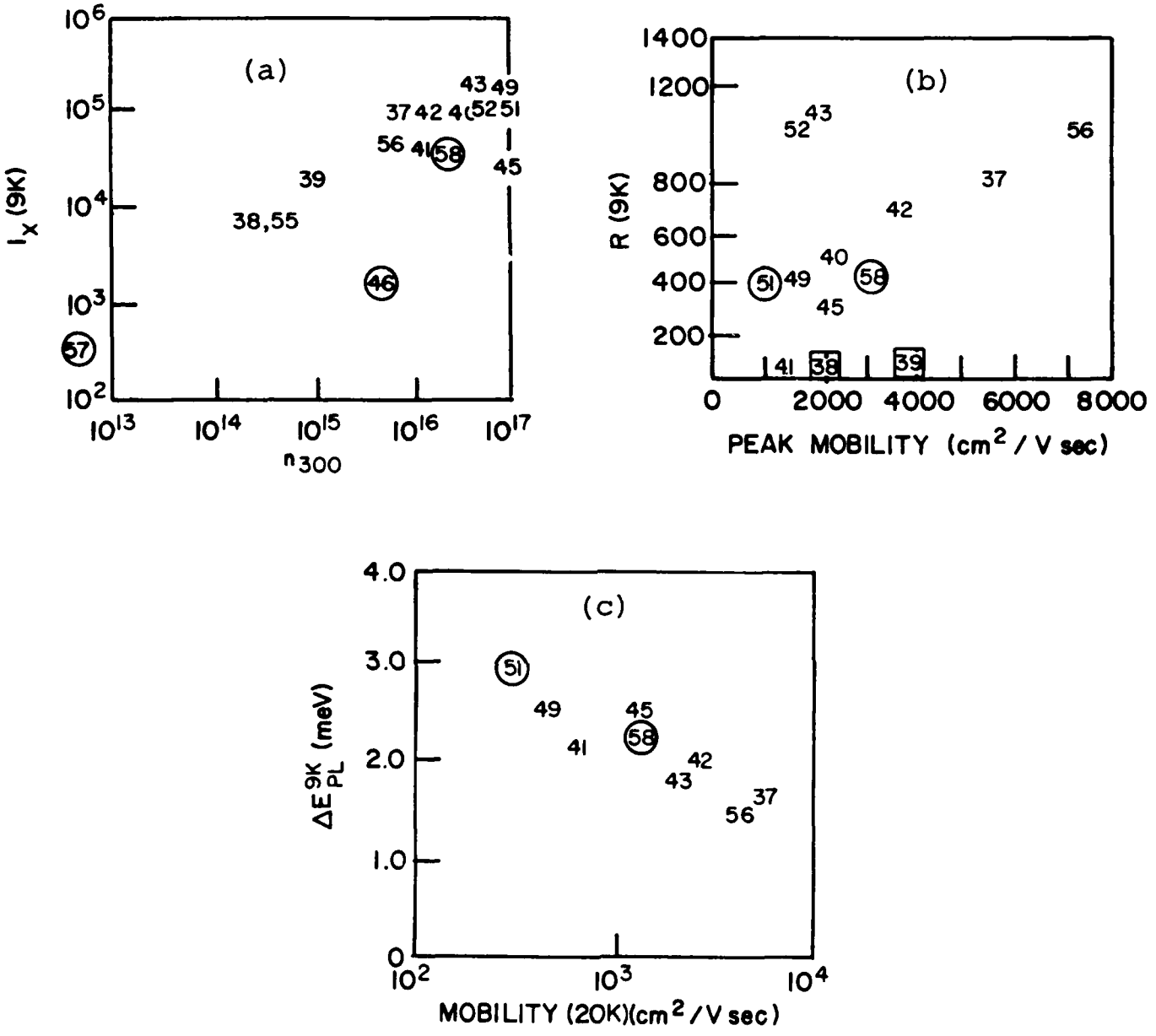

Figure 2-4. (a) Correlation plot showing the relationship between the 9K peak PL emission intensity and the room-temperature carrier concentration. Data points are the sample numbers. Circled numbers indicate samples from the corners of the growth matrix. Squares indicate 400°C data.
(b) Correlation diagram showing the relationship between the 9K R-value (NBE intensity/DL intensity) and the peak carrier mobility.
(c) Correlation diagram showing the relationship between the linewidth of the dominant NBE emission peak, I_x, at 9K and the low-temperature (20K) electron mobility.

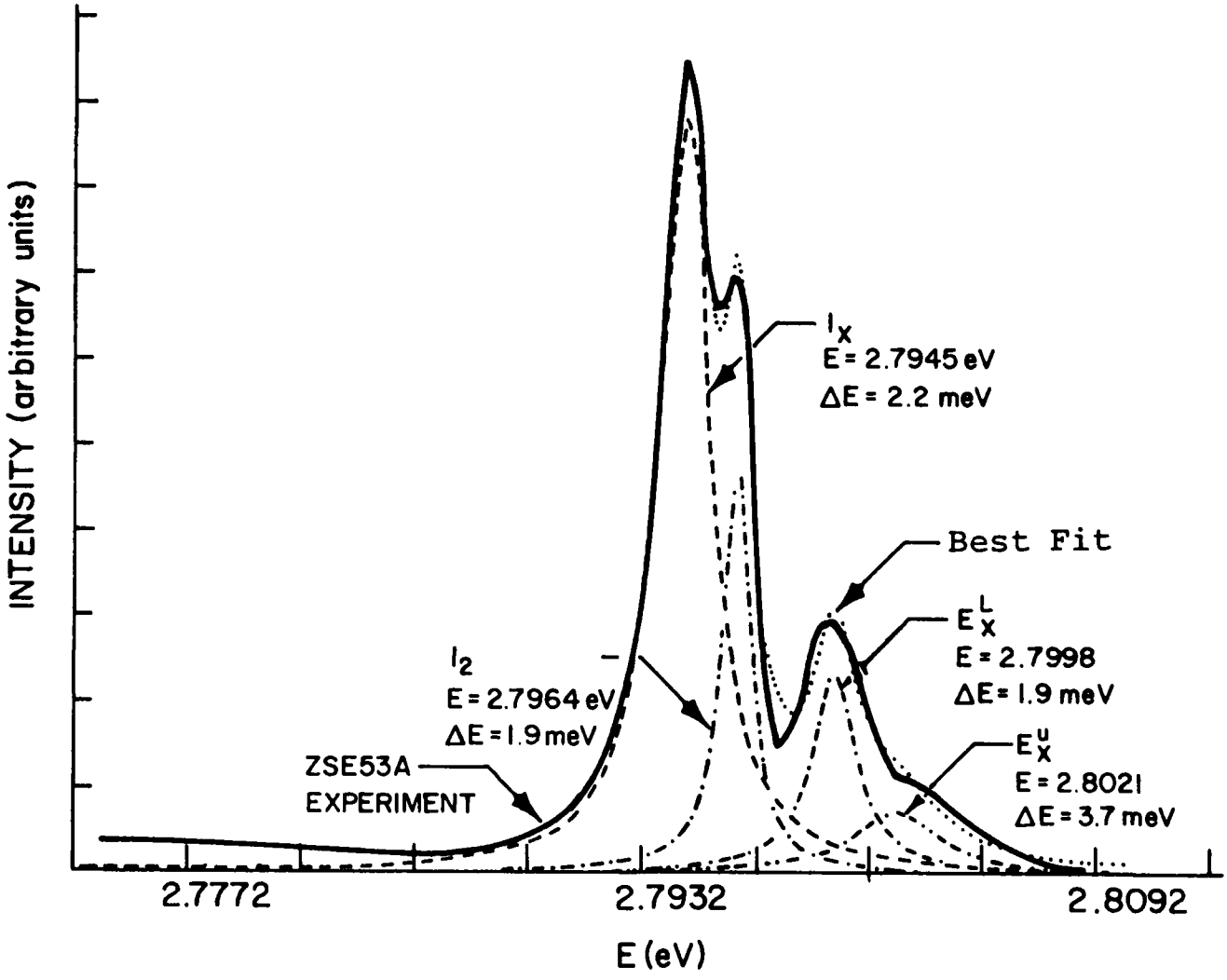

Figure 2-5. Demonstration of the spectral curve-fitting capability. The solid curve represents the original data for sample #ZSE53A, the dashed and dash-dot curves represent the four Lorentzian peaks which give a best fit to the data, and the dotted line is the sum of the four individual peaks.

2.1.1.3 Selective Excitation Photoluminescence and Raman Scattering of Unintentionally-Doped ZnSe on (100) GaAs

We have extended our SPL measurements on sample ZSE37A--one of our samples which showed the highest mobility and narrowest PL linewidths. As reported earlier, we observe two main features in the two-electron region: one narrow feature (open circles in the excitation spectrum, Figure 2-6) and a broader feature (solid dots in Figure 2-6), both of whose intensities exhibit maxima when the excitation line is at 22547 and 22563 cm^{-1}. These two features behave differently, however, when their energies are studied while varying the incident energy. In Figure 2-7 we see that the narrow feature (open circles) shifts linearly with the incident energy, indicating that this is a Raman scattering, rather than PL, peak. The dashed line fits the data to a Raman shift of 19.8 meV--a value corresponding to the 1S--2P energy of Cl donors [2]. At low incident energies ($E_{inc} < E(I_x)$, the data are better fit to a Raman shift of 19.3 meV, which would correspond to a Cl 1S--2S transition. We are currently trying to understand why the 2P transition would become favored over 2S for $E_{inc} > E(I_x)$. By contrast, the energy of the broader feature (solid dots) rises with the incident energy for $E_{inc} < E(I_x)$, but becomes independent of E_{inc} beyond that point. It appears that this is a case where Raman scattering evolves into PL when the latter process becomes energetically allowed [3]. As for identifying the species giving rise to this peak, the fit to the low-E_{inc} points yields a Raman shift of 18.4 meV. The PL position (22399.6 cm^{-1}) is displaced from the I_2 parent line by 20.4 meV and from the I_x parent line by 18.2 meV. No known hydrogenic donors have a 1S--2S splitting as small as 18.2 meV [2], while 20.4 meV does correspond to the 1S--2P splitting of the Ga donor states. We believe that this feature is due to Ga donors; we are currently trying to explain the details of the peculiar behaviors exhibited in Figures 2-6 and 2-7. It is noteworthy that there is evidence from these SPL measurements for the participation of both Ga and Cl in the I_x peak as well as in I_2. It may well be that these two peaks have the same origin, but represent donors in different environments in the film (e.g., sensing different local strain fields.) This work is being prepared for presentation at the SPIE Conf. "Modern Optical Characterization Techniques for Semiconductors and Semiconductor Devices" in March, 1987.

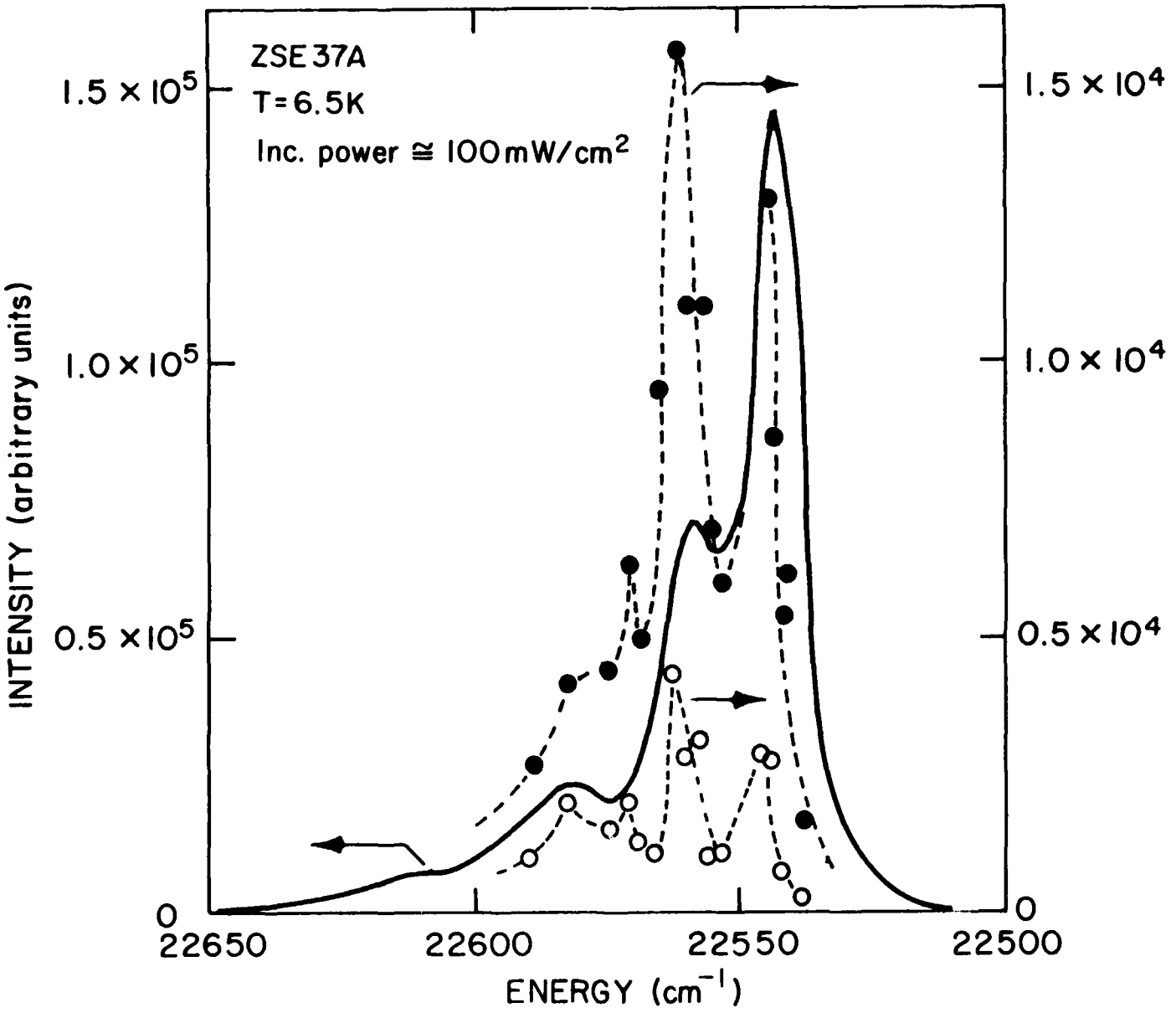

Figure 2-6. Selective excitation PL results for Sample #ZSE37A. The solid curve is the NBE emission spectrum obtained with above-bandgap radiation. When the sample is excited with radiation at these energies, two features are seen in the two-electron transition region. The intensity of the narrower of these two features is represented by the open circles, and the broader feature by the solid dots on this plot. These data have not been corrected for the sample absorption.

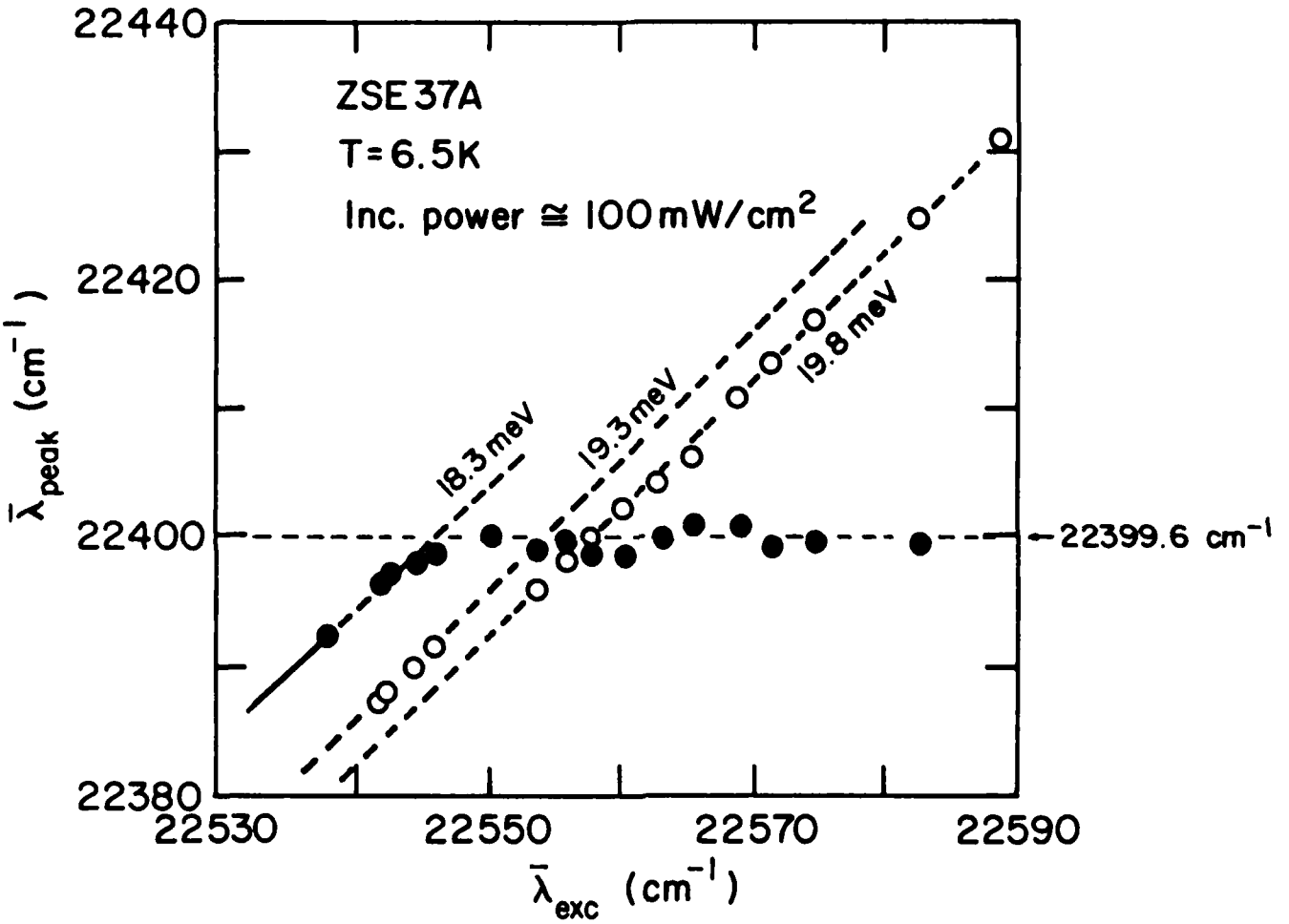

Figure 2-7. Selective excitation PL results for Sample ZSE37A. Shown are the energies of the two features seen in the two-electron region plotted as a function of the incident beam energy. Open circles: narrow feature. Solid dots: broad feature.

We have performed additional Raman scattering measurements on the interface (IF) phonon modes which we have observed in our thinnest films, and on which we have reported earlier [4]. The fact that we can observe phonons propagating in the xy plane while using a z( )$\bar{z}$ scattering geometry implies that wave-vector conservation has been destroyed, most likely by the presence of intrinsic defects or impurities. If so, we should be able to observe a resonance behavior for this scattering efficiency [5]. For this reason, we have measured the resonance behavior of the Raman scattering from these modes and from the ZnSe LO-phonon modes; these data are shown in Figure 2-8. The LO-phonon scattering exhibits a weak resonance when the incident photon is at the free-exciton energy (2.802 eV) and a stronger resonance when the outgoing photon is at the free-exciton energy (these data have not been corrected for absorption, so the resonance curve is distorted somewhat). By contrast, the IF mode scattering exhibits a sharp and strong resonance only when the incident photon is coincident with the I_x peak. This provides strong evidence for the participation of defect states--those defects which give rise to I_x--in the scattering process. A manuscript describing this work is currently being prepared.

2.1.1.4 Hall Measurements on Unintentionally-Doped ZnSe on (100) GaAs

Of the seven unintentionally-doped ZnSe films grown from October 1 through December 31, 1986, three were of extremely high resistivity and four were check runs related to the problem of substrate temperature control. Therefore, only results on the two samples comprising the growth rate study (ZSE66A and ZSE67A) will be reported here.

As mentioned previously, both of these samples were grown at 350°C with BPR = 1/4:1/2 for ZSE66A and BPR = 1/2:1 for ZSE67A. Under these conditions the growth rates for ZSE66A and ZSE67A were 0.5 and 0.9 microns/hour, respectively. The results of the Hall measurements for these two samples are shown in Figure 2-9. The room temperature carrier concentration in ZSE66A is slightly lower than the carrier concentration in ZSE67A. If we assume the compensation ratios to be identical for the two samples then the donor/acceptor concentration in ZSE66A is approximately 80% of the donor/acceptor concentration in ZSE67A:

N_D (ZSE66A) = 0.8 N_D (ZSE67A)

N_A (ZSE66A) = 0.8 N_A (ZSE67A).

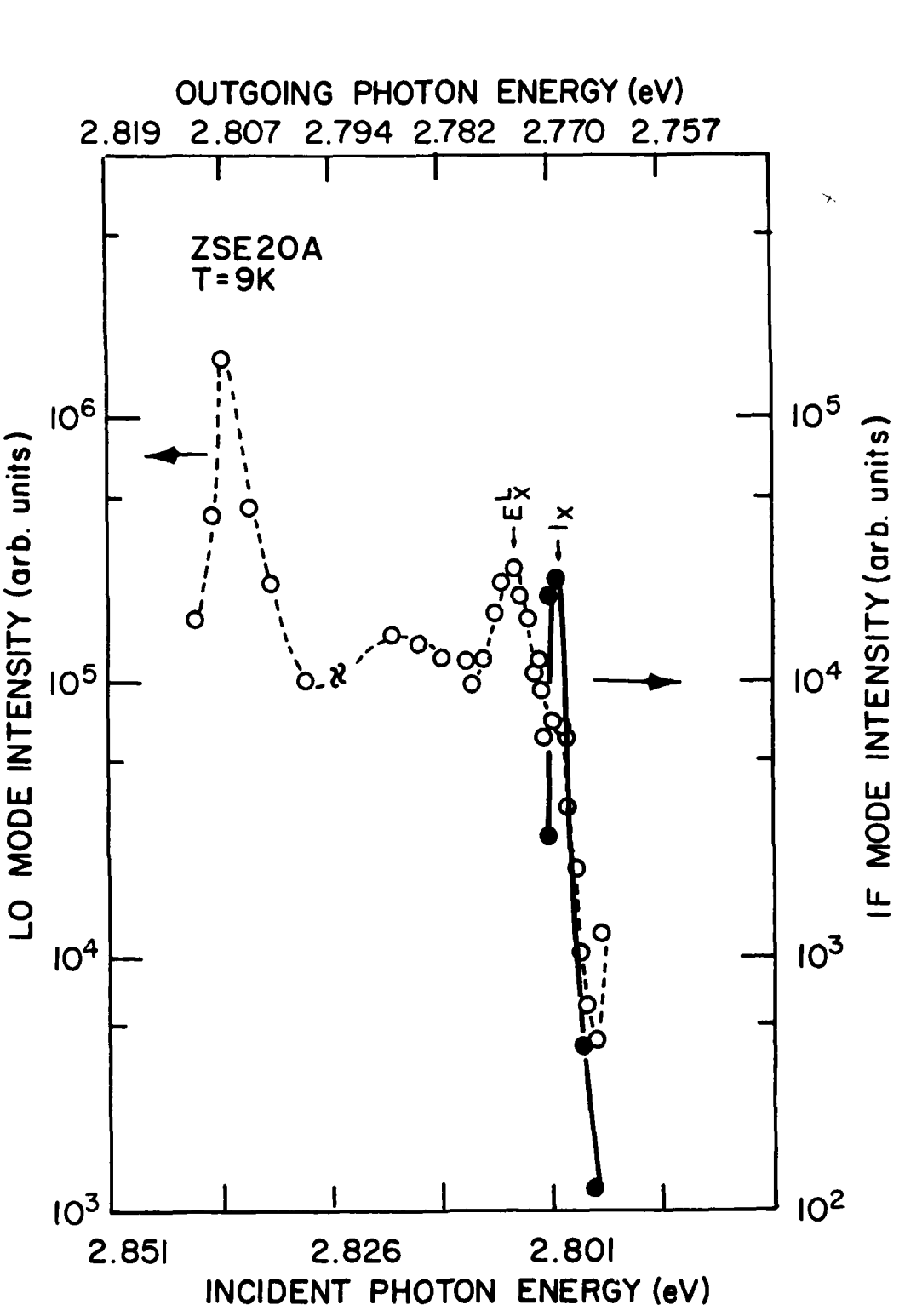

Figure 2-8. Resonance curve showing the intensity of the Raman scattering peak vs. incident photon energy for the ZnSe interface phonon mode (I_F: solid dots) and the LO-phonon mode (LO: open circles).

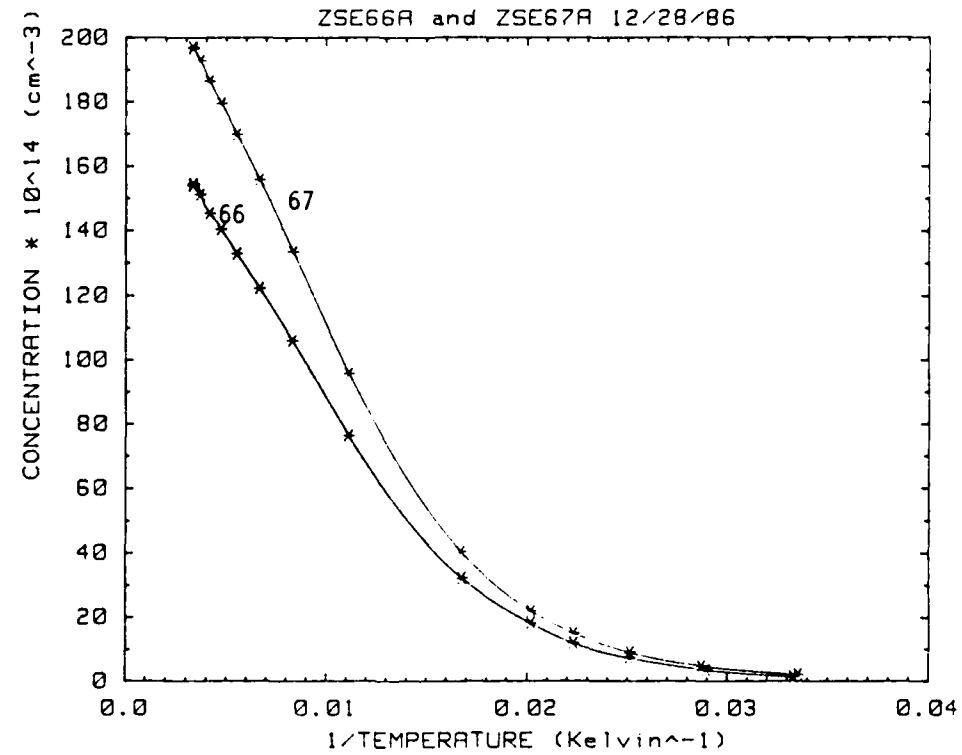

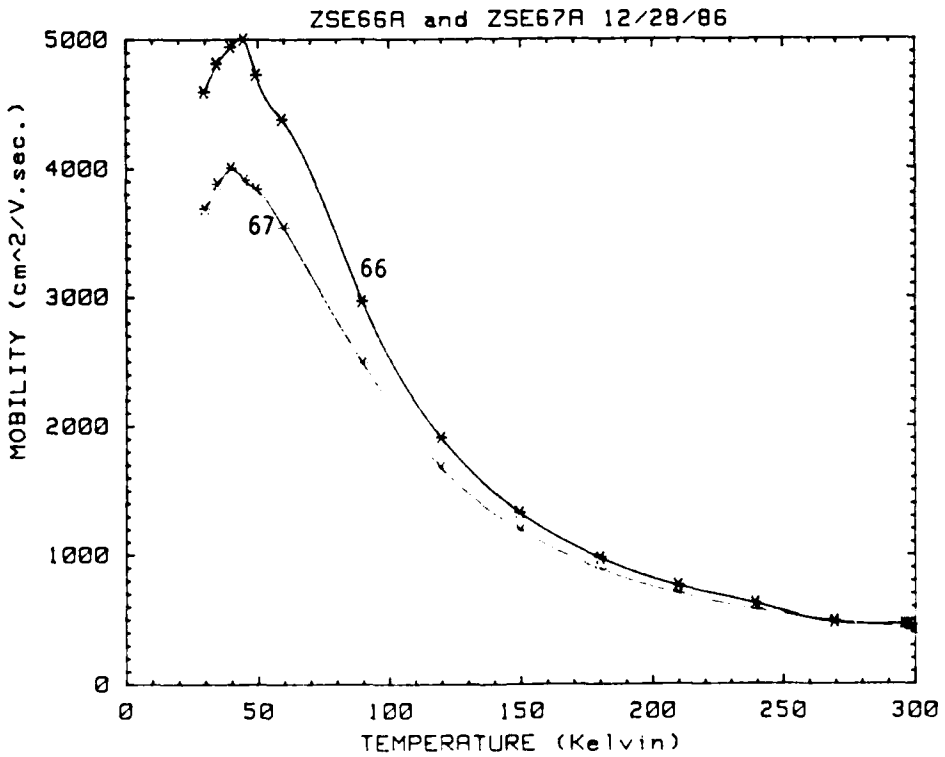

Figure 2-9. Electron concentrations and mobilities for samples in the growth rate study. Both samples were grown with T_g = 350° C, and BPR = 1/2:1. Sample ZSE66 was grown at a rate of 0.5 microns/hour and Sample ZSE67 was grown at a rate of 0.9 microns/hour, to approximately the same total thickness.

Similar conclusions are reached by considering the measured peak mobilities. The peak mobility of ZSE67A is approximately 80% of the peak mobility in ZSE66A. If we assume that the difference in peak mobility between these two samples is determined by the difference in the number of ionized impurities (assuming all other major scattering mechanisms are sample independent), then, since mobility due to ionized impurity scattering varies roughly as the inverse of the ionized impurity concentration, this again indicates the ionized impurity concentration in ZSE66A to be about 80% of that in ZSE67A.

We may conclude that the growth rate does affect the unintentional incorporation of donors and acceptors in ZnSe, but the influence of the growth rate, however, is modest.

2.1.1.5 Capacitance Spectroscopy of Unintentionally-Doped ZnSe on (100) GaAs

In the last quarterly report we used Shah and Reddi's model [6] to analyze the frequency dependence of the capacitance of metal/ZnSe/n^+ GaAs structures. A value of $N_T \phi_T$ (N_T = trap concentration and ϕ_T = trap depth) of 1.0×10^{16} was obtained from the low frequency C-V measurements. In order to do emission rate and trap depth measurements, we carried out temperature and frequency dependent measurements of sample capacitance. Such a measurement is shown in Figure 2-10. Based on Fermi level or emission rate effects, one would expect an increase in capacitance with increasing temperature. This is observed in Figure 2-10 for $\omega < 100$ kHZ. For $\omega > 100$ kHZ, the capacitance goes through a maximum and decreases with temperature. For comparison we have measured the temperature dependence of the capacitance of GaAs Schottky barriers grown in our laboratory. These showed a systematic increase in capacitance with temperature as expected. The results obtained for ZnSe are probably due to poor interface characteristics. In order to reduce the interface layer thickness, we have done the following: i) sputter deposition of the contacts, and ii) chemical treatment of ZnSe surface prior to contact deposition.

Sputtered contacts were made by sputtering gold through a mask onto ZnSe using a diode sputtering system. Current-voltage characteristics of sputtered Au on ZnSe indicated sputter-induced damage.

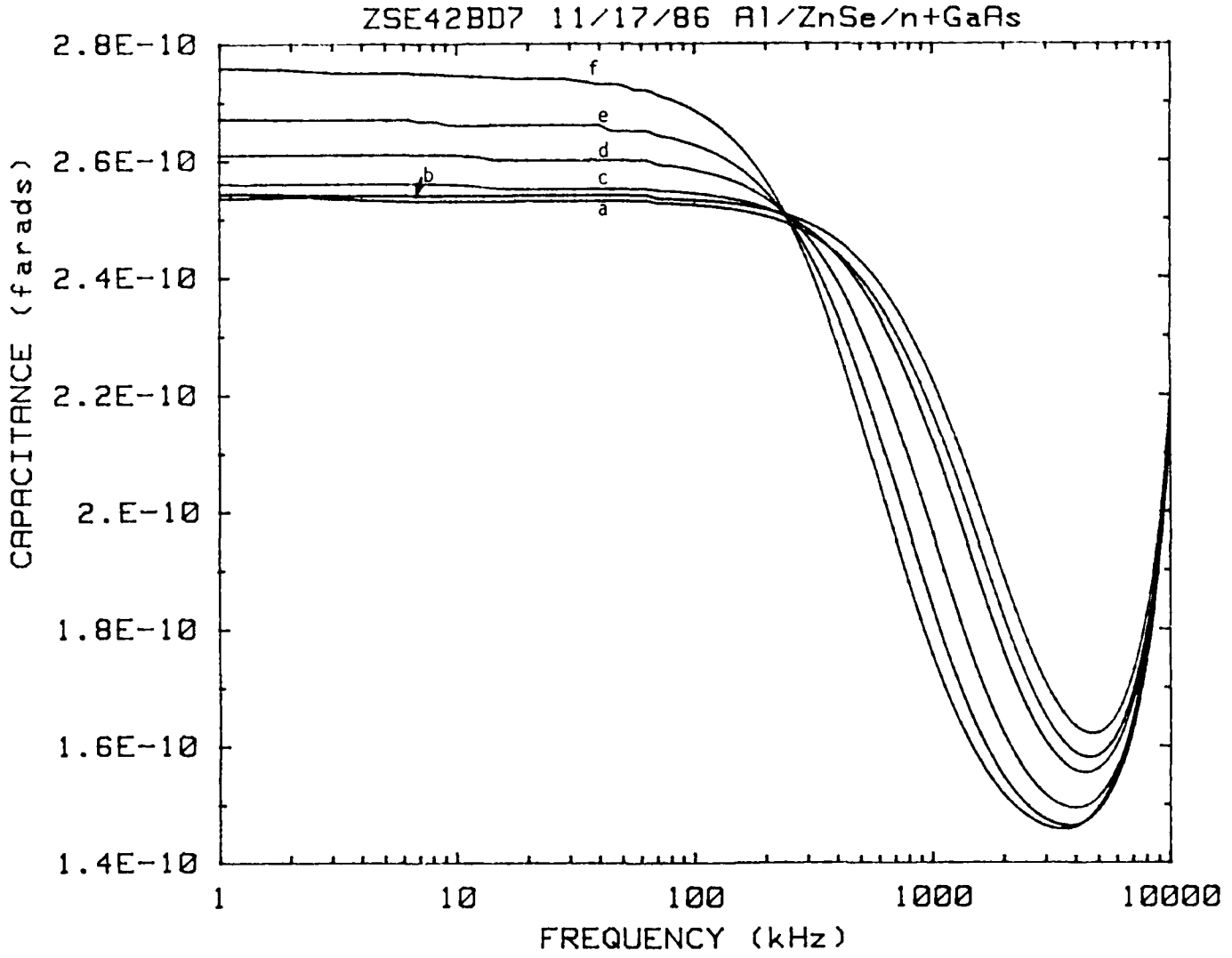

Figure 2-10. Frequency dependent zero bias capacitance of ZnSe.
a) 80 K, b) 100 K, c) 150 K, d) 200 K, e) 250 K, f) 300K

Annealing of the contact after sputtering might be a way to reduce the ion induced damage, but we have postponed systematic annealing studies due to time constraints.

Studies of the effects of chemical treatment were made to determine whether the quasi-static low frequency capacitance shown in Figure 2-10 is due to interface states or to bulk traps consistent with the Shah-Reddi model. Capacitance-voltage (C-V) and current-voltage measurements were made on ZnSe samples with evaporated aluminum and gold Schottky barriers. The various chemical treatments given to the ZnSe samples are summarized as follows: i) untreated; ii) degreased in tricholorethylene, acetone and methanol; iii) degreased and treated in boiling water; iv) etched in KOH at 90°C. $1/C^2$ vs. V plots for some typical samples are shown in Figure 2-11, and I-V characteristics are shown in Figure 2-12. C-V measurements showed a faster saturation of $1/C^2$ vs. V in forward bias for the ZnSe sample treated in boiling water; I-V characteristics indicated somewhat higher forward current and reverse leakage current for that sample. Differences were also noted in the frequency dependence of the capacitance; these are shown in Figures 2-13 and 2-14. Both the figures indicate identical high frequency zero bias capacitance values, whereas the capacitance varied 10-20% for low frequencies ($\omega < 50$ kHZ), depending on the surface treatment. This relative change in capacitance is attributed to a change in surface state density due to chemical treatment. This makes it difficult to fabricate reproducible Schottky barriers on ZnSe without <u>in situ</u> contact layer deposition after epitaxial growth.

During the process of our surface treatment studies we have also observed some variability in carrier concentration profiles due to surface treatment. This is shown in Figure 2-15 for an untreated ZnSe/n^+ GaAs sample and for a sample treated with $K_2Cr_2O_7:12H_2SO_4:1H_2O$ and KCN. The purpose of this chemical treatment was to reduce the surface oxide [7]. About 20% variation in concentration profile is observed in our results. This variation may be due to spatial non-uniformity in the carrier concentration, or to variation in the interfacial layer between the metal and the semiconductor.

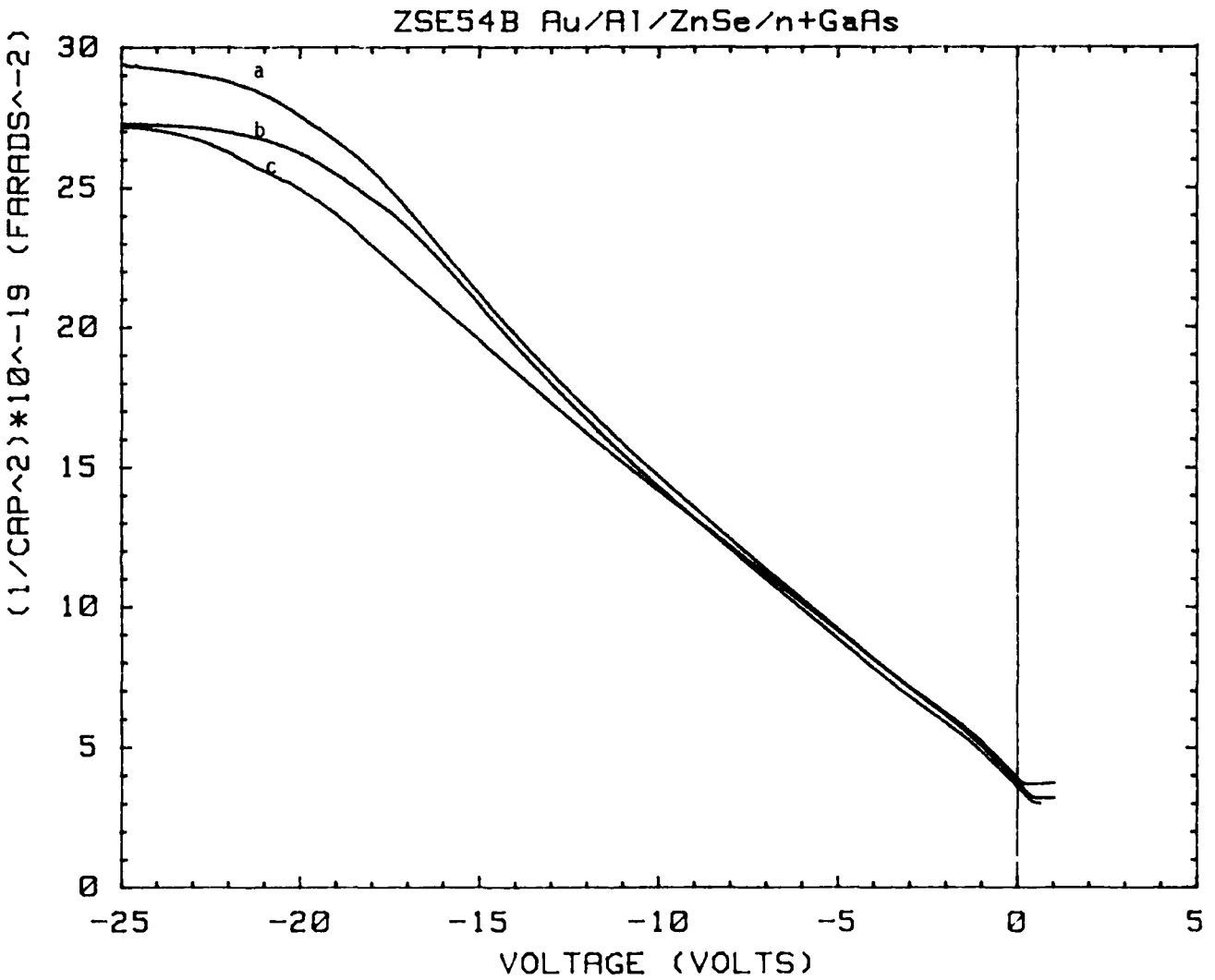

Figure 2-11. $1/C^2$ vs. voltage for chemically treated ZnSe Schottky barrier diodes (SBD's): a) standard (untreated), b) degreased and treated in boiling water, c) degreased.

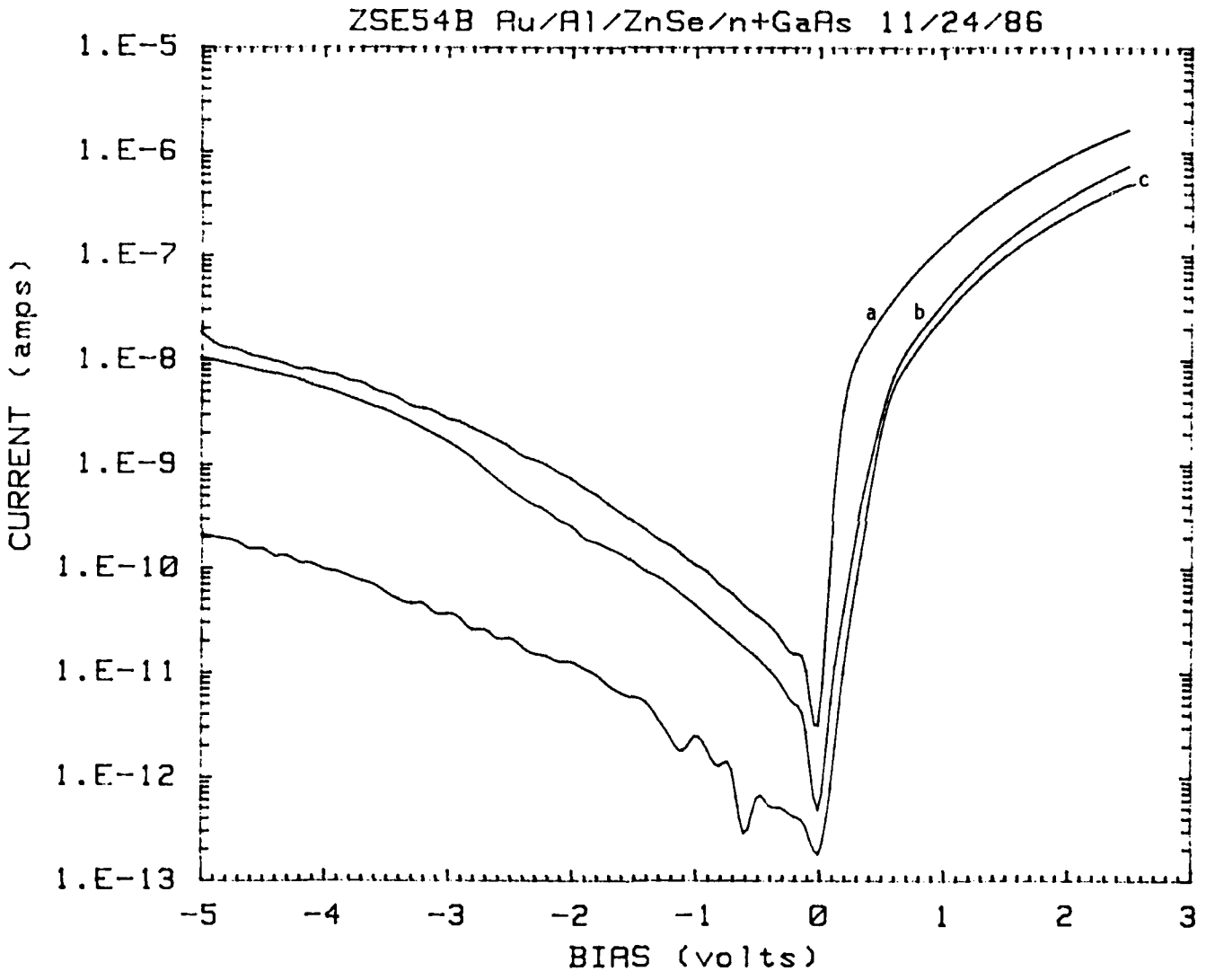

Figure 2-12. Current-voltage characteristics of chemically-treated ZnSe SBD: a, b, and c as in Figure 2-11.

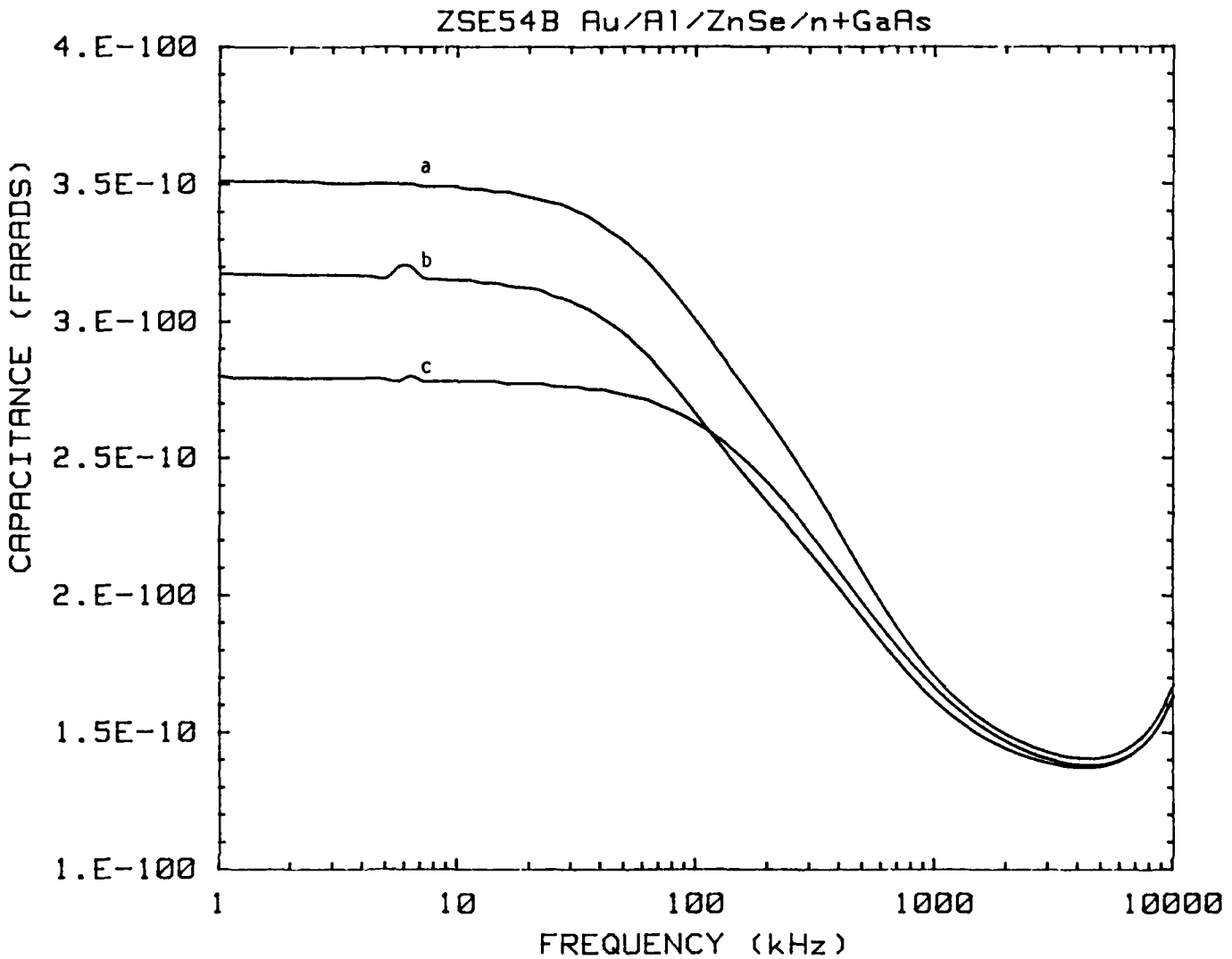

Figure 2-13. Capacitance-frequency characteristics of ZnSe SBD: a, b, and c as in Figure 2-11.

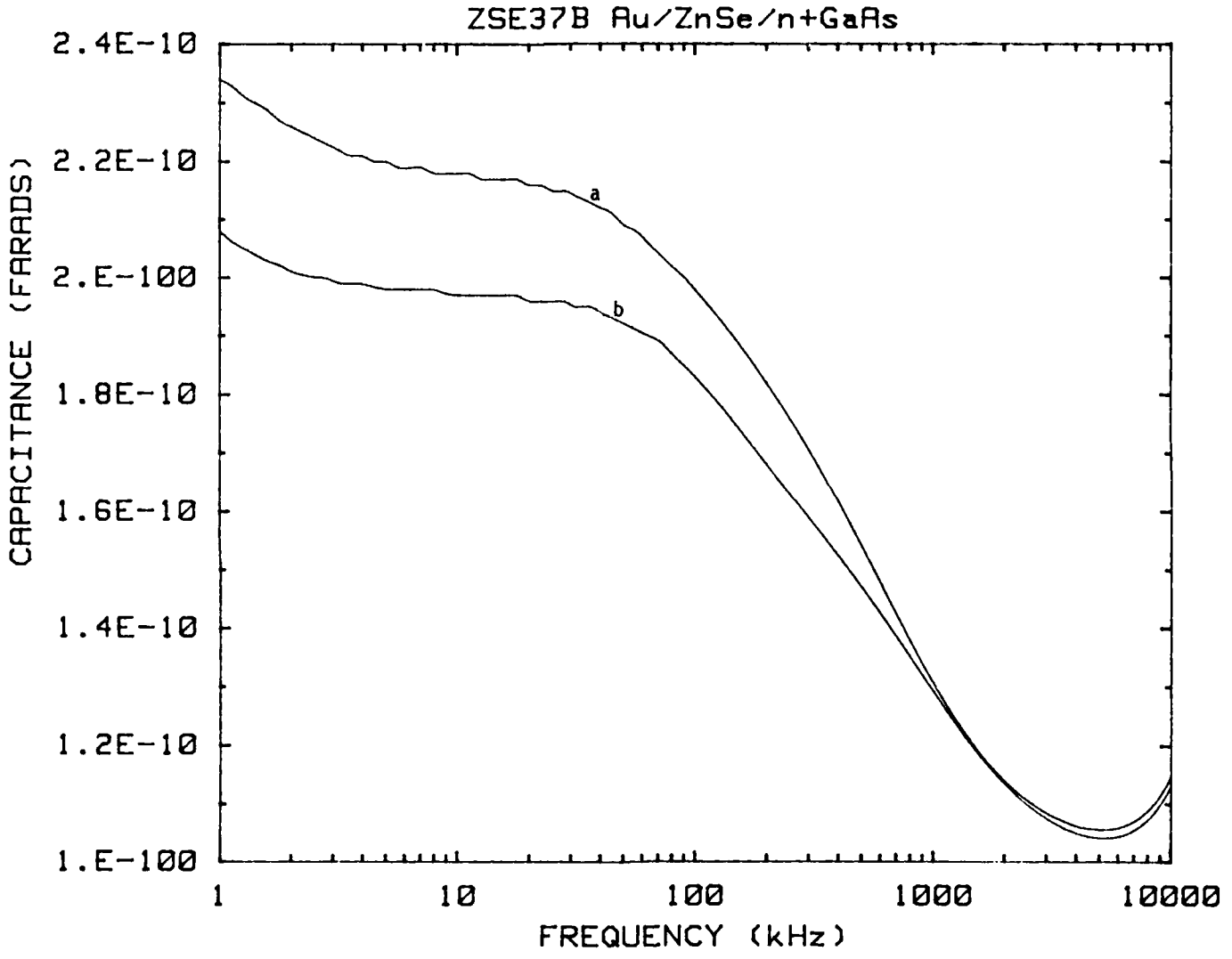

Figure 2-14. Capacitance-frequency characteristics of ZnSe SBD: a) standard, b) degreased, and treated in KOH (90°C, 2 minutes).

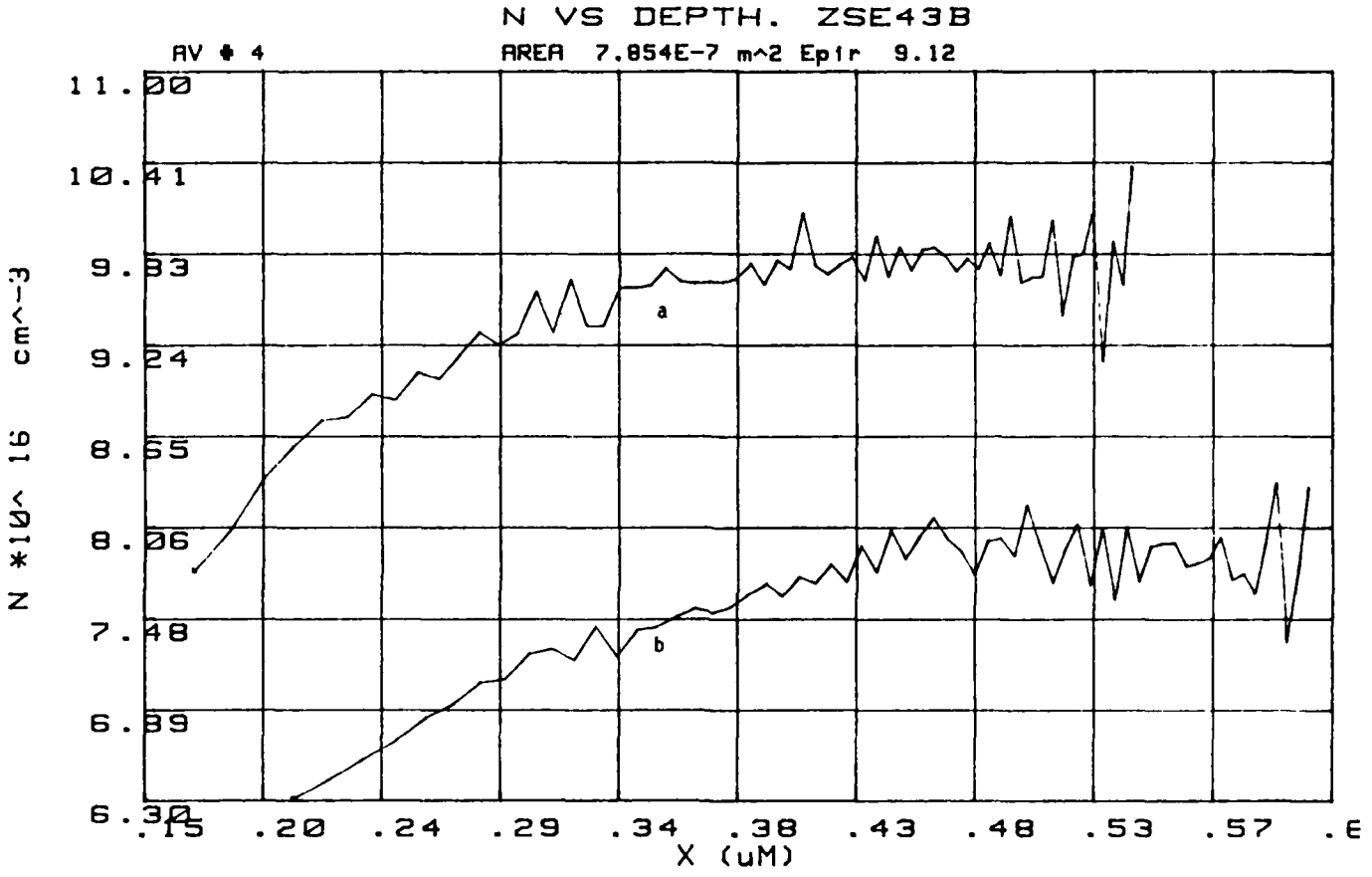

Figure 2-15. Carrier concentration profile in ZnSe SBD: a) standard b) with surface treatment.

In order to avoid problems associated with interfacial layers, we have started some preliminary work in M-I-S structure fabrication on ZnSe using evaporated organic PTCDA (3,4,9,10 - Perylenetetracarbonxylic dianhydride) as an insulator. This has several advantages: e.g. the organic can be completely removed after the C-V measurement, and high reverse bias can be used to deplete the semiconductor for complete carrier profiling information. Concentration profiling for ZSE42B using PTCDA as the insulator is shown in Figure 2-16. More work will be carried out to determine the usefulness of this approach.

2.1.2 X-Ray Double Crystal Rocking Curve Comparative Studies of ZnSe/GaAs and ZnSe/Ge

Careful DCRC analysis of both ZnSe/GaAs and ZnSe/Ge layers grown by MBE with a substrate orientation, 2° off (100) → [110] has revealed two principal findings: firstly, the linewidths of the (400) ZnSe reflections are a function of the angular position of the sample and, secondly, the ZnSe layers are misoriented with respect to the substrate orientation.

The first finding is illustrated in Figures 2-17 (a) and (b). The DCRC linewidths recorded from ZnSe/GaAs and ZnSe/Ge layers grown at three substrate temperatures, namely, 310, 330 and 350°C to a thickness of 2 μm are shown in Figure 2-17 (a). The bars drawn in the figure are not error bars but, in fact, correspond to the range of DCRC linewidths recorded from each layer as a function of angular position of the sample with respect to the X-ray beam, each sample being rotated through a full 360° in the sample plane. Figure 2-17 (b) shows a second example of this phenomenon and is a plot of the DCRC linewidths recorded from ZnSe/GaAs and ZnSe/Ge layers grown to various thicknesses under a fixed set of growth conditions, namely, a Zn to Se beam pressure ratio of unity together with a substrate temperature of 330°C. Again the bars in the figure do not represent error bars but rather the range of DCRC linewidths recorded as a function of angular position of the sample.

In addition to the observed dependence of the DCRC linewidth on angular position, a variation in the separation between the layer and substrate (400) peaks was also observed on rotation of the sample in its own plane with respect to the fixed X-ray beam, indicating misorientation of the layer with respect to the substrate.

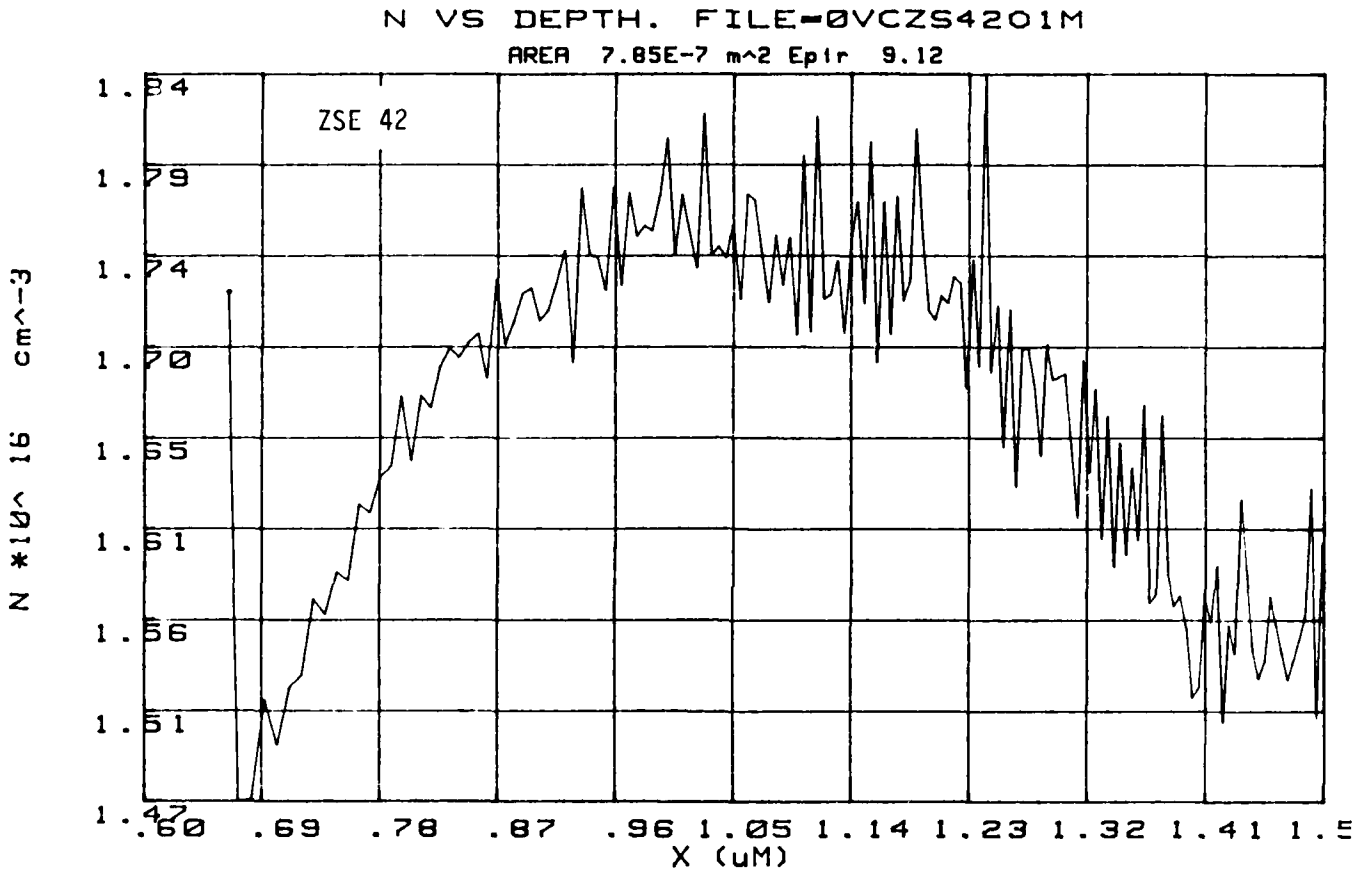

Figure 2-16. Carrier concentration profiling in ZnSe using In/organic/ZnSe/n^+ GaAs structure.

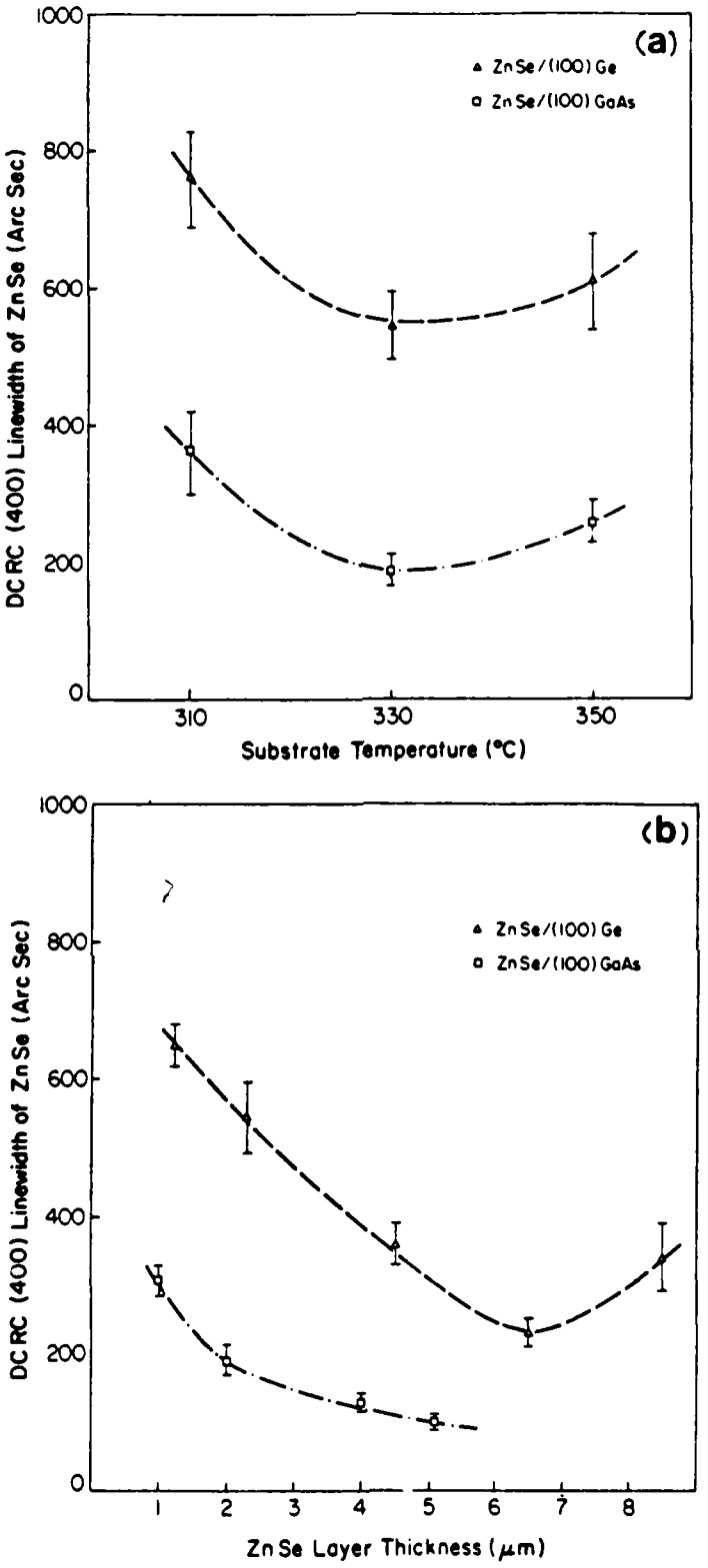

Figure 2-17. Double crystal rocking curve (DCRC) (400) linewidth data recorded from ZnSe/GaAs and ZnSe/Ge layers grown (a) at three substrate temperatures to a thickness of 2 μm and (b) under an identical set of growth conditions to various thicknesses. The bars correspond to the range of linewidths recorded for each layer as a function of angular position of the sample.

The peak separation dependence on angular position was more pronounced for ZnSe/Ge layers. Moreover, the sign of the peak separation was observed to move from positive to negative and back to positive on full 360° rotation of the sample for (ZnSe/Ge layers) indicative of a high degree of tilt of the layer with respect to the substrate.

Figures 2-18 (a) and (b), show the layer and substrate (400) peak separations plotted as functions of angular position for typical ZnSe/GaAs and ZnSe/Ge samples, respectively. The tilt angle (layer with respect to substrate orientation), $\Delta\phi$, and the lattice mismatch, $\Delta\Theta$, can be estimated from such measurements, as illustrated in Figure 2-18. As can be seen from the figure, the ZnSe/Ge layer has a much larger tilt angle (~ 960") than the ZnSe/GaAs layer (~ 40").

As mentioned above, the peak separation for ZnSe/Ge layers was observed to exhibit a sign change on a full rotation of the sample. This observation is illustrated in Figure 2-19. The DCRC spectra showing both substrate (narrow peaks) and layer (broad peaks) (400) reflections recorded at 45° intervals from 0 to 360° are shown in the figure. Such a dependence of peak separation on angular position (α) of the sample can be explained in the following manner with reference to the diagram in Figure 2-19. Two cones representing Bragg conditions for the substrate (S) and the layer (F) are shown to be misoriented by an angle $\Delta\phi$ = 00'. On rotation of such a system about the α axis, the substrate and layer (400) peak separation will change. As can be readily seen from the figure, a large misorientation results in a situation whereby the layer cone lies partially outside the substrate cone and consequently, the peak separation can exhibit a sign change on a full 360° rotation of the sample. [For each angular position the sample was rocked about the ω axis following optimization of signal intensity achieved by adjustment about the x axis.]

A consequence of the above results is that the standard technique of determining tilt and mismatch by recording two DCRC spectra separated by 180° is not appropriate for large misorientations and, in fact, will lead to erroneous results. A full rotation of the sample is required in such cases in order to estimate $\Delta\phi$ and $\Delta\Theta$ as shown in Figure 2-18.

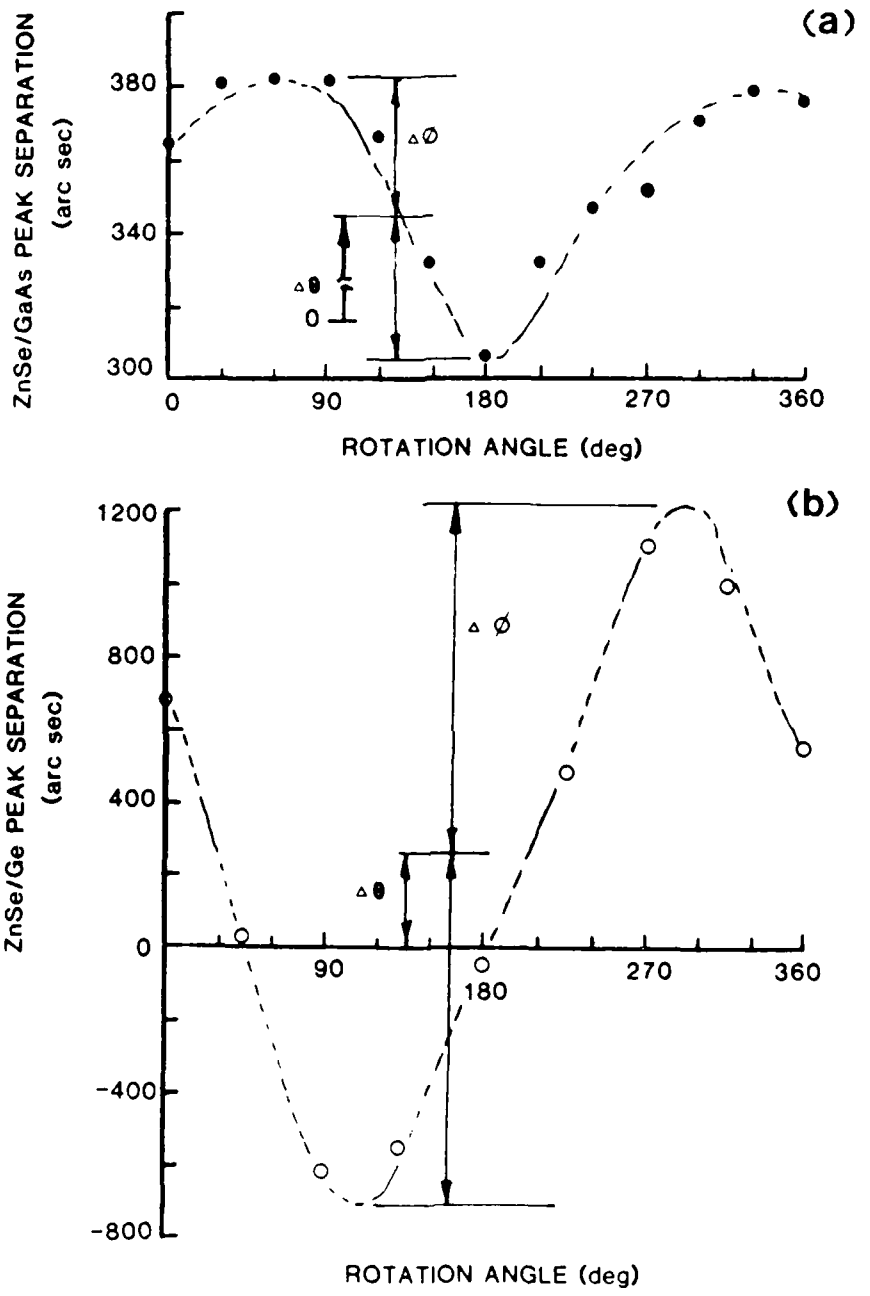

Figure 2-18. Layer and substrate (400) peak separation plotted as a function of angular position of the sample for (a) a typical ZnSe/GaAs sample and (b) a typical ZnSe/Ge sample.

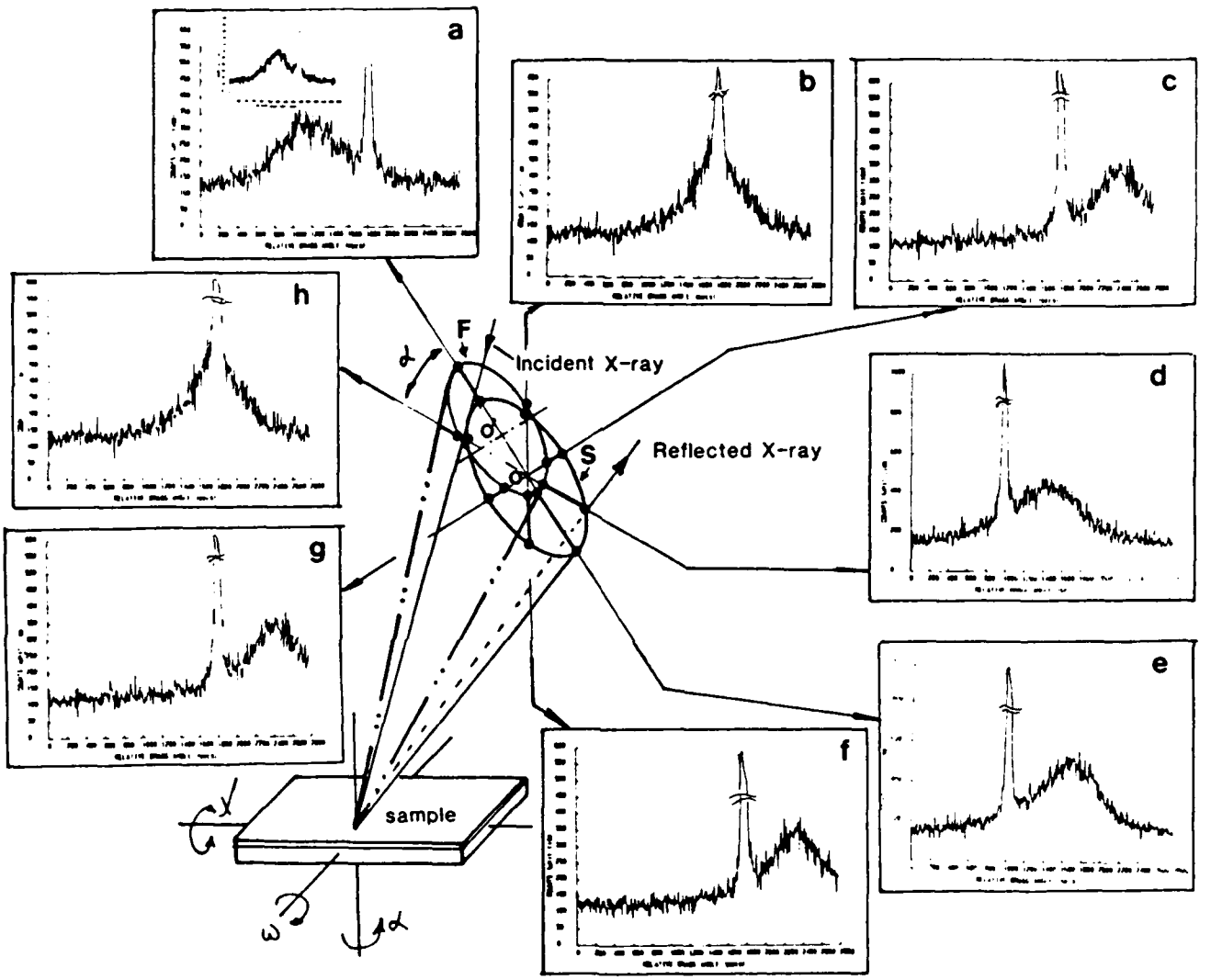

Figure 2-19. Angular position dependence of layer and substrate (400) peak separation for a ZnSe/Ge sample. Note the peak separation sign change moving in a clockwise direction from (a) to (h), indicative of a large tilt angle of the layer with respect to the substrate.

2.1.3 Unintentionally-Doped ZnSe on Si with ZnSe/Ge Superlattice Buffer Layers

An exploratory investigation was carried out into the incorporation of ZnSe/Ge superlattice buffers as a means of improving the quality of ZnSe layers grown on Si substrates.

ZnSe/Ge superlattices were grown on sputtered and annealed (100) Si substrates by alternately opening and closing Zn and Se, and Ge K-cell shutters, the substrate temperature being held constant at 330°C. The ZnSe and Ge epi-layer growth rates for the K-cell temperatures selected were ~ 0.5 μm/hour and ~ 0.33 μm/hour, respectively. ZnSe and Ge alternate epi-layer deposition was indicated by RHEED pattern observations. Figures 2-20 (a), (b), (c), (d), (e), and (f) show the RHEED patterns recorded at a fixed azimuth from first the Si substrate and then alternate layers of Ge and ZnSe. In this case the ZnSe and Ge epi-layers were ~ 300 Å in thickness. As can be seen from the figure, the (2 x 2) surface reconstructed, streaky Ge pattern was obtained from each Ge epi-layer despite the fact that the ZnSe layers exhibited rather rough surfaces on the atomic scale. It should be noted that when deposition of extremely thin alternate layers was attempted, namely around 60 Å thickness, a polycrystalline RHEED pattern quickly developed. It is therefore concluded that there is some minimum alternate layer thickness for the ZnSe/Ge system to maintain epitaxy.

To date, 2 μm thick ZnSe layers have been grown on two-period and ten-period ZnSe/Ge superlattices on Si. The ZnSe layer quality achieved by incorporating both two- and ten-period superlattices was compared to that obtained by growing ZnSe directly on Si using SEM, TEM and 4.2K PL characterization techniques.

Figures 2-21 (a), (b), and (c) illustrate the surface morphologies observed in the SEM from layers grown (a) directly on Si, (b) with a ten-period superlattice buffer, and (c) with a two-period superlattice buffer. As can be seen from the figure the smoothest surface was obtained by the incorporation of the two-period superlattice.

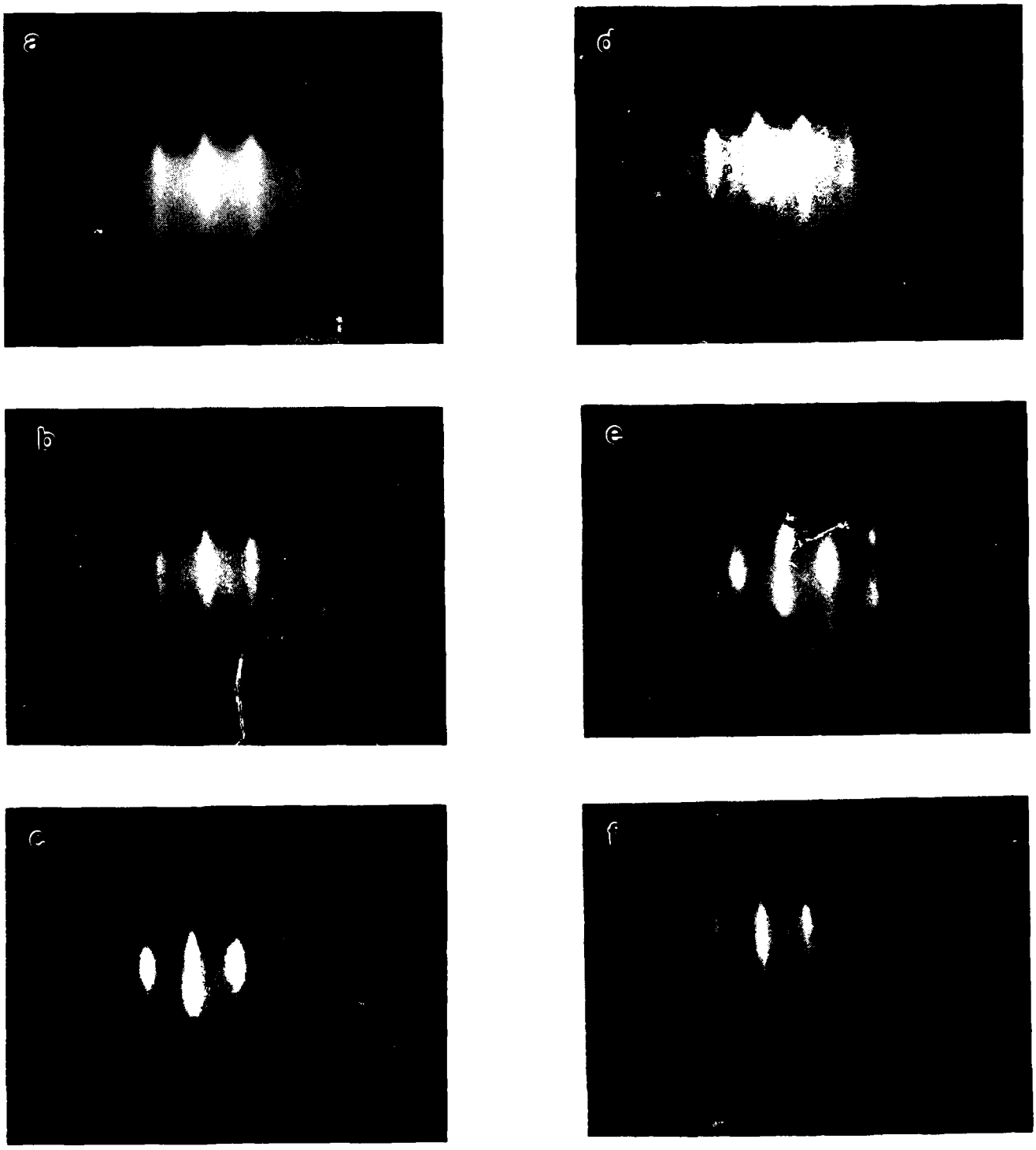

Figure 2-20. RHEED patterns recorded in the $(1\bar{1}0)$ azimuth during the growth of a ZnSe/Ge superlattice on Si.
(a) sputtered/annealed (100) Si substrate pattern.
(b) First 300 Å thick Ge layer.
(c) First 300 Å thick ZnSe layer.
(d) Second 300 Å thick Ge layer.
(e) Second 300 Å thick ZnSe layer.
(f) Third 300 Å thick Ge layer.

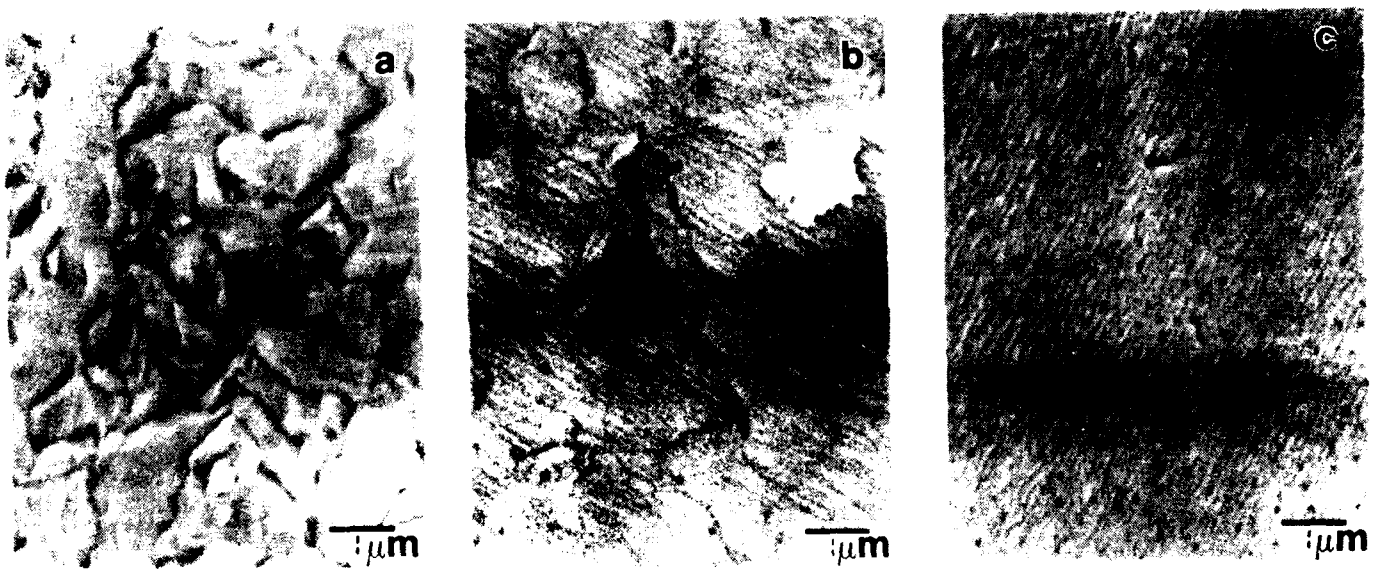

ZnSe/Si ZnSe/10 PERIOD SUPERLATTICE/Si ZnSe/2 PERIOD SUPERLATTICE/Si

Figure 2-21. SEM micrographs of surface morphologies of ZnSe layers grown directly on Si and with superlattice buffers incorporated.

A further indication of layer quality improvement due to the incorporation of a two-period superlattice was suggested by cross-sectional TEM analysis. Figures 2-22 (a) and (b) show cross-sectional TEM micrographs recorded from ZnSe layers grown on a ten-period SL and a two-period SL, respectively, As can be seen from Figure 2-22 (b) the ZnSe layer grown on the two-period SL is of excellent quality, with essentially only twin defects being observed. In contrast, the layer grown on the ten-period SL contains additional structural defects including stacking faults.

Finally, Figures 2-23 (a) and (b) illustrate 4.2K PL spectra recorded from ZnSe layers grown directly on Si, and with a two-period SL buffer incorporated, respectively, As can be seen from Figure 2-23 (a), the PL spectrum obtained from a layer grown directly on Si is dominated by the defect related Y_o emission peak, in contrast to the dominant bound-excitonic emission recorded from the layer grown on a two-period SL buffer. Also, as can be seen from Figure 2-23 (b) the defect related Y_o peak is barely detectable from this layer. The detailed excitonic spectra shown in Figures 2-24 (a) and (b) also show a marked contrast. Figure 2-24 (a) which shows a very broad excitonic emission peak shifted considerably to lower energies was recorded from a ZnSe layer grown directly on Si. On the other hand, a quite narrow bound-exciton peak (~ 2 meV linewidth), as shown in Figure 2-24 (b), was observed from the layer grown on the two-period SL, indicating the achievement of much higher quality material. The PL spectra recorded from layers grown on a ten-period SL showed little or no improvement over those recorded from layers grown directly on Si.

2.1.4 SIMS Analyses

During this quarter, SIMS efforts were concentrated on attempts to develop standard analysis conditions for Na, F, Cl, and N, using ion-implanted standards. These efforts resulted in obtaining a quantitative calibration for Na, which was used to determine the Na concentration in Na doping experiments.

Efforts to obtain calibrations for F, Cl, and N were less successful than for Na, since large background signals were found for all three of these elements.

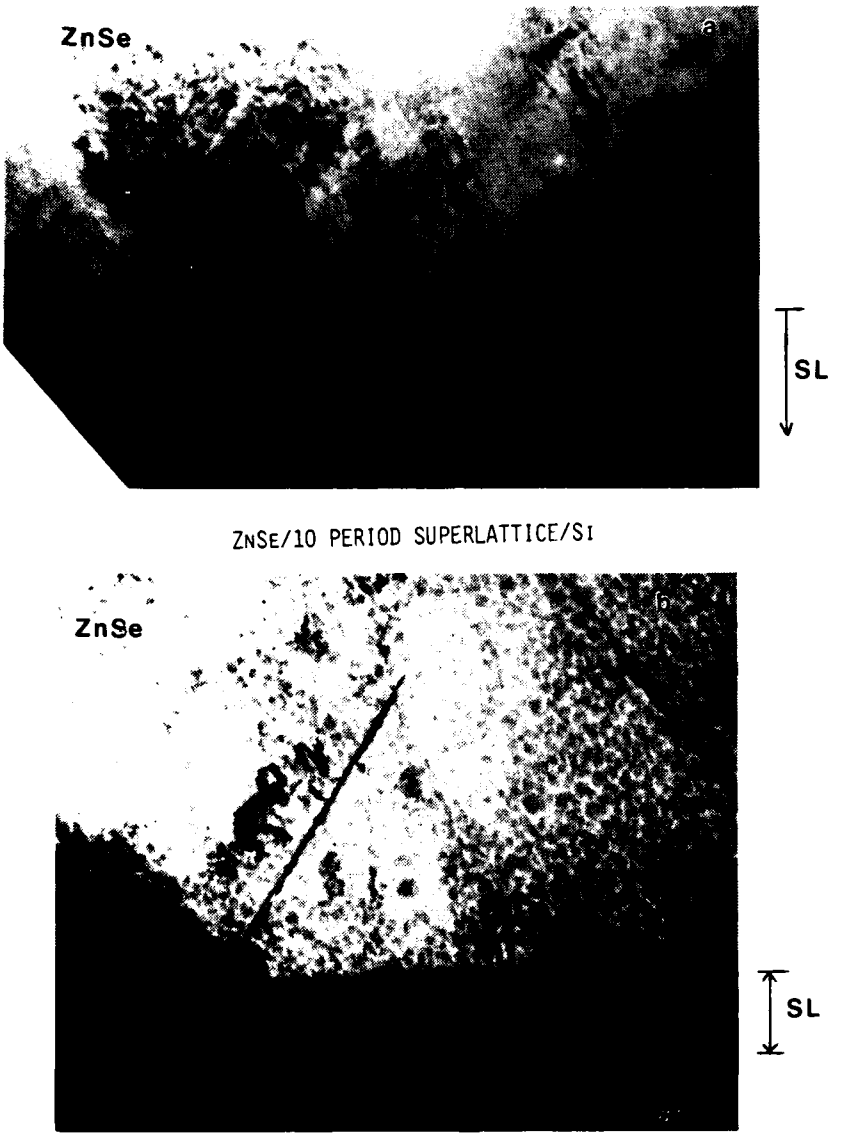

Figure 2-22. Cross-sectional TEM micrographs recorded from ZnSe/superlattice/Si structures.

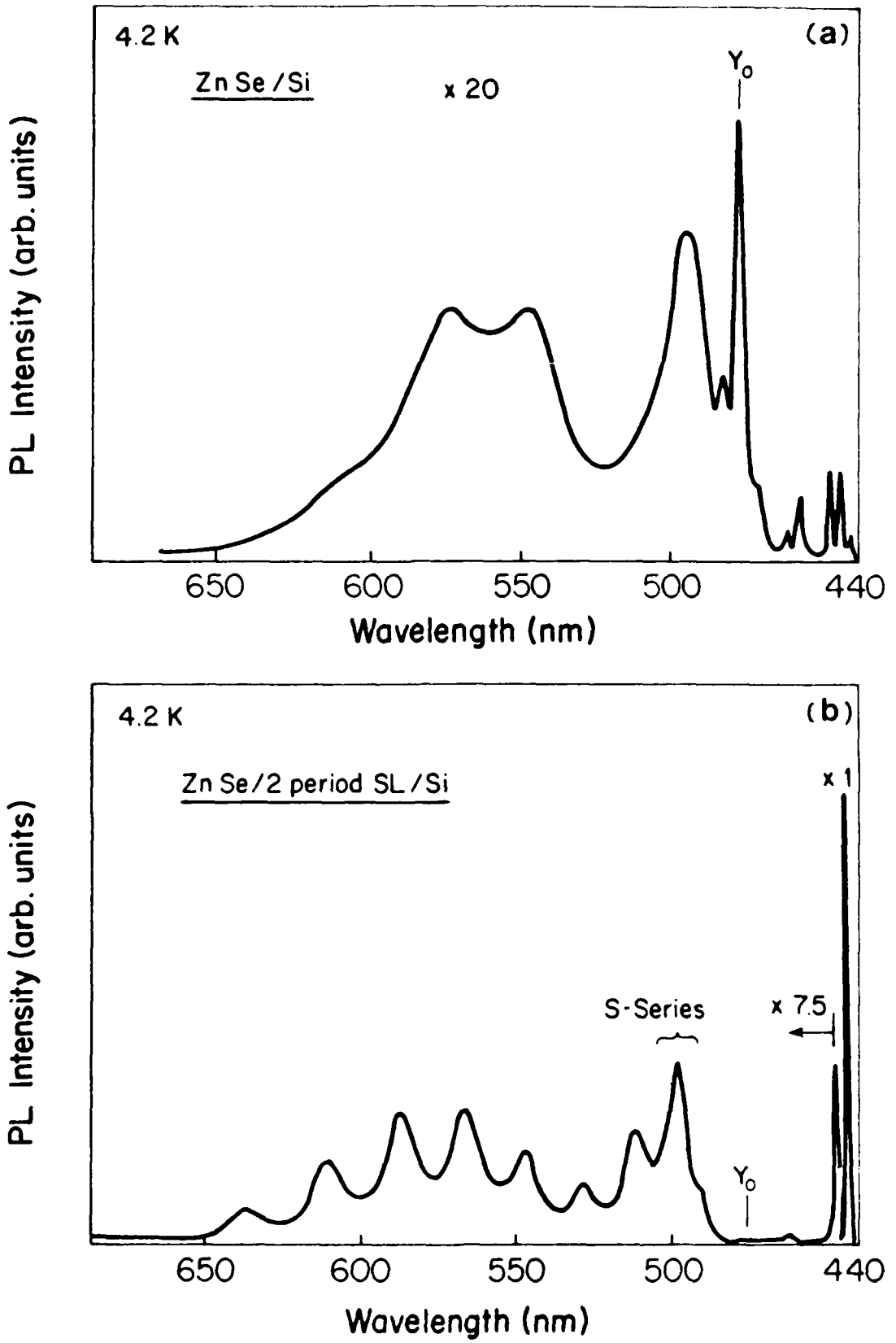

Figure 2-23. 4.2K PL spectra recorded from (a) ZnSe grown directly on Si and (b) ZnSe grown on Si with a two-period superlattice buffer incorporated.

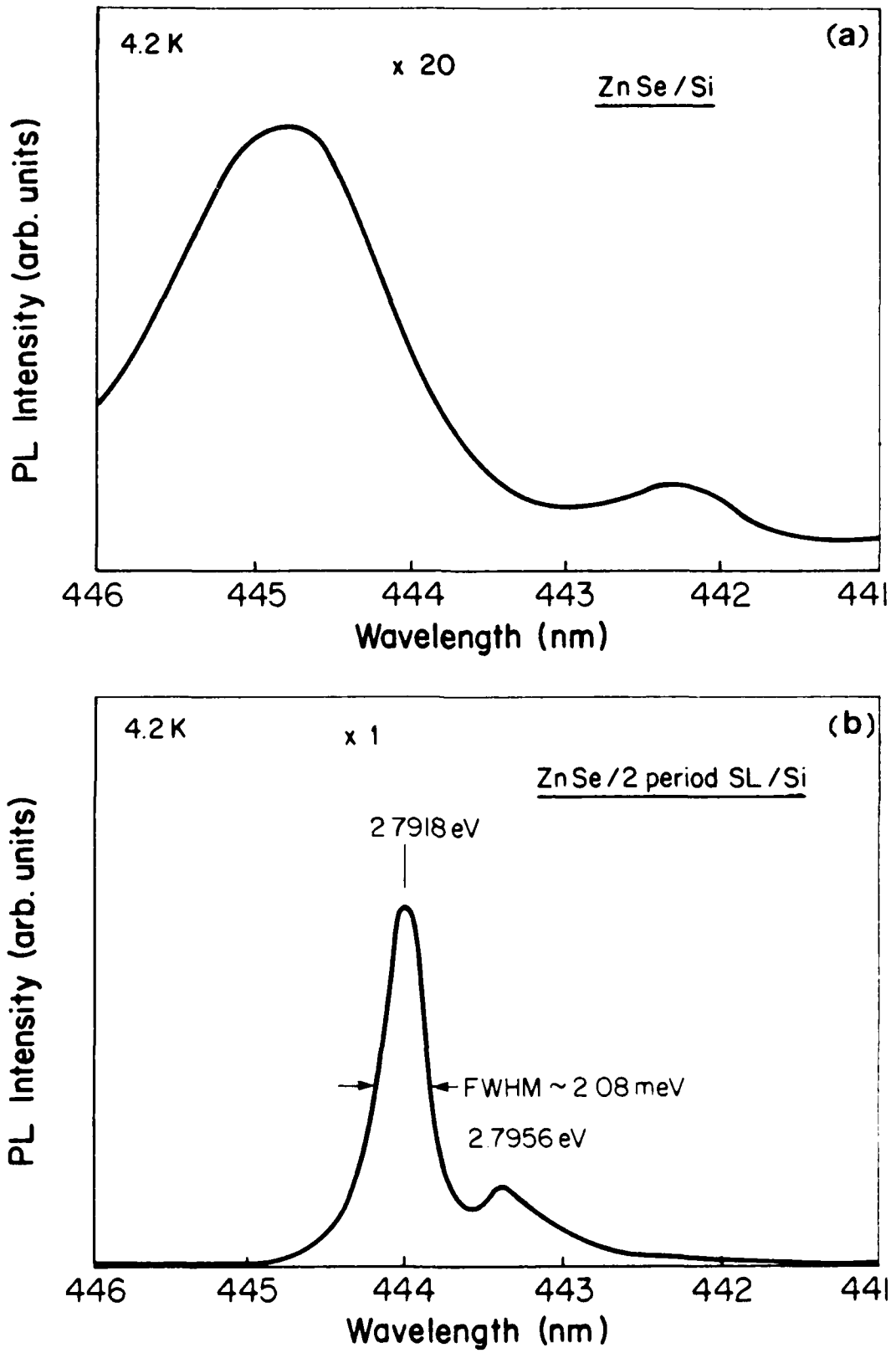

Figure 2-24. 4.2K PL excitonic spectra recorded from (a) ZnSe grown directly on Si and (b) ZnSe grown on Si with a two-period ZnSe/Ge superlattice buffer incorporated.

Table 2.1 summarizes the detection limits found to date in studies of various different ion-implanted species. Here the "statistical limit" is defined as the concentration giving the minimum usable secondary ion count rate under the constraints imposed by the sample volume available for analysis, in the absence of interference. This is taken to be 1 c/s at maximum primary beam current. The "background limit" is defined as the concentration corresponding to the experimentally observed background count rate (usually > 1 c/s) under the same conditions. The statistical and background limits quoted here are for machine parameters required to minimize suspected interferences. Note that although the intrinsic sensitivity for F, Cl, and even N detection is high (as indicated by the small statistical limit), the large background signal raises the minimum detectable concentration to 5 x 10^{16} cm^{-3} (2 ppm) in all three cases. Attempts to use the voltage offset technique to increase the observed peak-to-background ratios for F, Cl, and N implanted samples were unsuccessful, indicating that the background signals are probably not due to molecular interference, but rather are due to contamination of the SIMS vacuum system (or of the implanted ZnSe) with these elements. Efforts to determine the origin of, and if possible, reduce, the large background signals, are currently underway.

TABLE 2.1 SIMS Detection Limits.

Element	Statistical Limit (x 10^{15} cm^{-3})	Background Limit (x 10^{15} cm^{-3})
Al	0.1	0.1
Ga	0.04	2.0
In	0.02	0.2
Na	0.04	2.0
F	0.05	50.0
Cl	0.02	50.0
N	0.02	50.0

Also this quarter, ion-implanted standard samples were produced for B, C, O, and P, but these have not yet been analyzed. Unfortunately, a large amount of SIMS machine time was lost this quarter due to problems experienced with the stability of the magnet in the mass spectrometer. Efforts to solve this problem are continuing.

2.2 Project 1, Task 2: Materials Research - p-ZnSe

Efforts began this quarter to produce p-ZnSe by incorporation of acceptors into high-quality unintentionally-doped material. The St. Paul group began studies of Na acceptors, using an effusion cell loaded with Na_2Se as the Na source. The Toronto group studied N acceptors, using a leak valve to bleed gaseous N_2 into the growth chamber. Both groups observed evidence of acceptor levels in photoluminescence spectra, but electrical measurements showed n-type conduction.

2.2.1 Na-Doped ZnSe on (100) GaAs

Samples ZSE69 to ZSE73 were the first attempts made by the St. Paul group at Na doping. The Na dopant was supplied by heating Na_2Se powder (specified to be 3 9's purity) in one effusion cell. The Na_2Se powder was prepared for the growth run by first ramping the oven temperature gently to 450°C, then outgassing for two hours. This resulted in the evolution of a large amount of water vapor, which is not surprising since the fine Na_2Se powder reacts rapidly with moisture in the air, changing from white to reddish in a matter of minutes.

2.2.1.1 ZnSe:Na Growth Procedures and SIMS Results

The doping studies were performed in two subsets. In the first, the ZnSe growth parameters were kept constant, namely a substrate temperature of 350°C and a BPR of 1/2:1, while the Na_2Se oven temperature was varied to produce different Na fluxes. In the second subset, the Na_2Se oven temperature was held constant at 450°C while the substrate temperature and BPR were varied to study the relationship between growth conditions and Na incorporation. Growth conditions for the Na-doping attempts to date are summarized in Table 2.2. Also presented are SIMS determinations of the incorporated Na concentration. Only sample ZSE71 and ZSE73 showed appreciable Na incorporation (the background in undoped samples corresponds to about 2×10^{15} cm^{-3}). In ZSE73 the Na concentration was constant through the thickness of the sample, while in ZSE71 the Na concentration decreased monotonically from 2×10^{17} cm^{-3} at the sample surface to 1×10^{16} cm^{-3} at the ZnSe/GaAs interface. This may indicate drift in the Na flux, possibly due to Na_2Se oven instability.

TABLE 2.2. Na Doping Parameters.

Sample #	Substrate Temperature (°C)	BPR	Na_2Se Oven Temperature (°C)	[Na] (x 10^{15} cm^{-3})	$[n]_{300}$ (x 10^{15} cm^{-3})
ZSE68	350	1/2:1	375	4.5	20
ZSE69	350	1/2:1	450	6.3	210
ZSE70	350	1/2:1	500	4.5	290
ZSE71	270	1/2:1	450	10-200	350
ZSE72	350	1:1	450	[illegible]	120
ZSE73	260	1:1	450	200	180

During the growth of samples at substrate temperatures of 350°C and BPR = 1/2:1, it was noticed that as the Na_2Se was heated from 375°C to 500°C, the RHEED pattern changed from the typical streaky pattern [Figure 2-25 (a)] to a strange pattern [Figure 2-25 (b)] consisting of spots and crosses. This may indicate a rough, faceted surface; in the future, SEM studies will be performed to check this.

2.2.1.2 ZnSe:Na Photoluminescence

We have measured the PL spectra for the series of films (ZSE68-ZSE73) grown in an attempt to introduce p-doping using a Na_2Se source. Figure 2-26 shows a representative spectrum for one of the samples (ZSE69A) grown in this series. For all of the samples in this series (except for the first one, ZSE68A, for which the temperature of the Na oven was only 375°C), one can clearly see the incorporation of significant amounts of Na as evidenced by the appearance of donor-acceptor pair (DAP) spectra near 2.7 eV. In sample ZSE69A, for example, we find a DAP series with its zero-phonon peak at 2.7132 eV and an intensity $I_{DAP} = 0.4X\ I_x$.

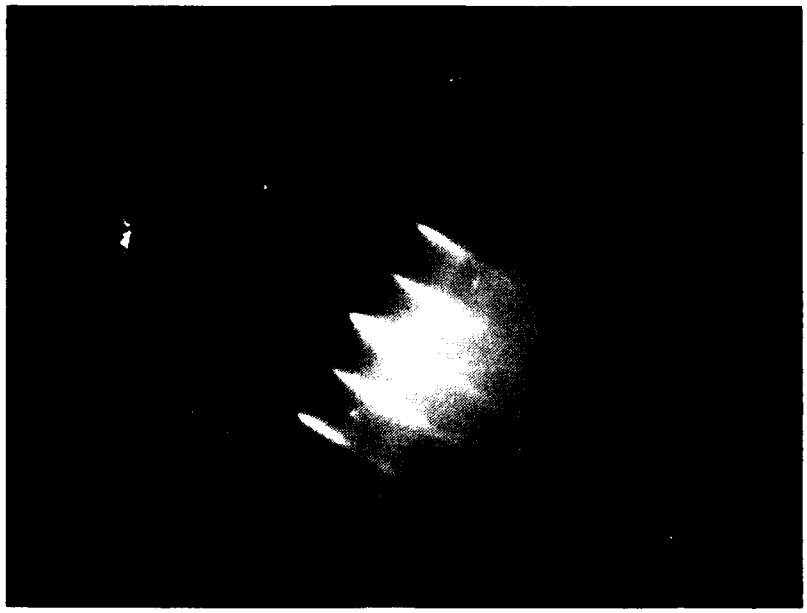

(a)

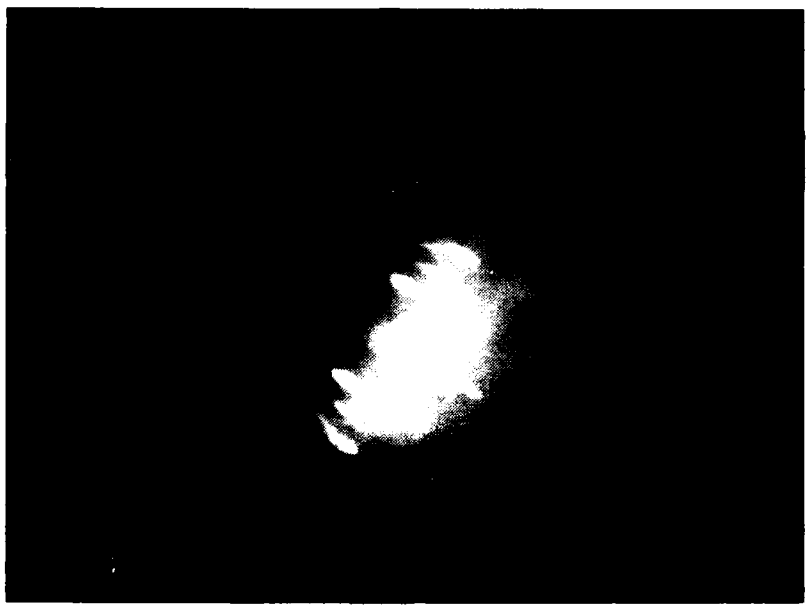

(b)

Figure 2-25. RHEED patterns of growing (100) ZnSe surface with Na_2Se oven temperature at (a) 375°C and (b) 500°C.

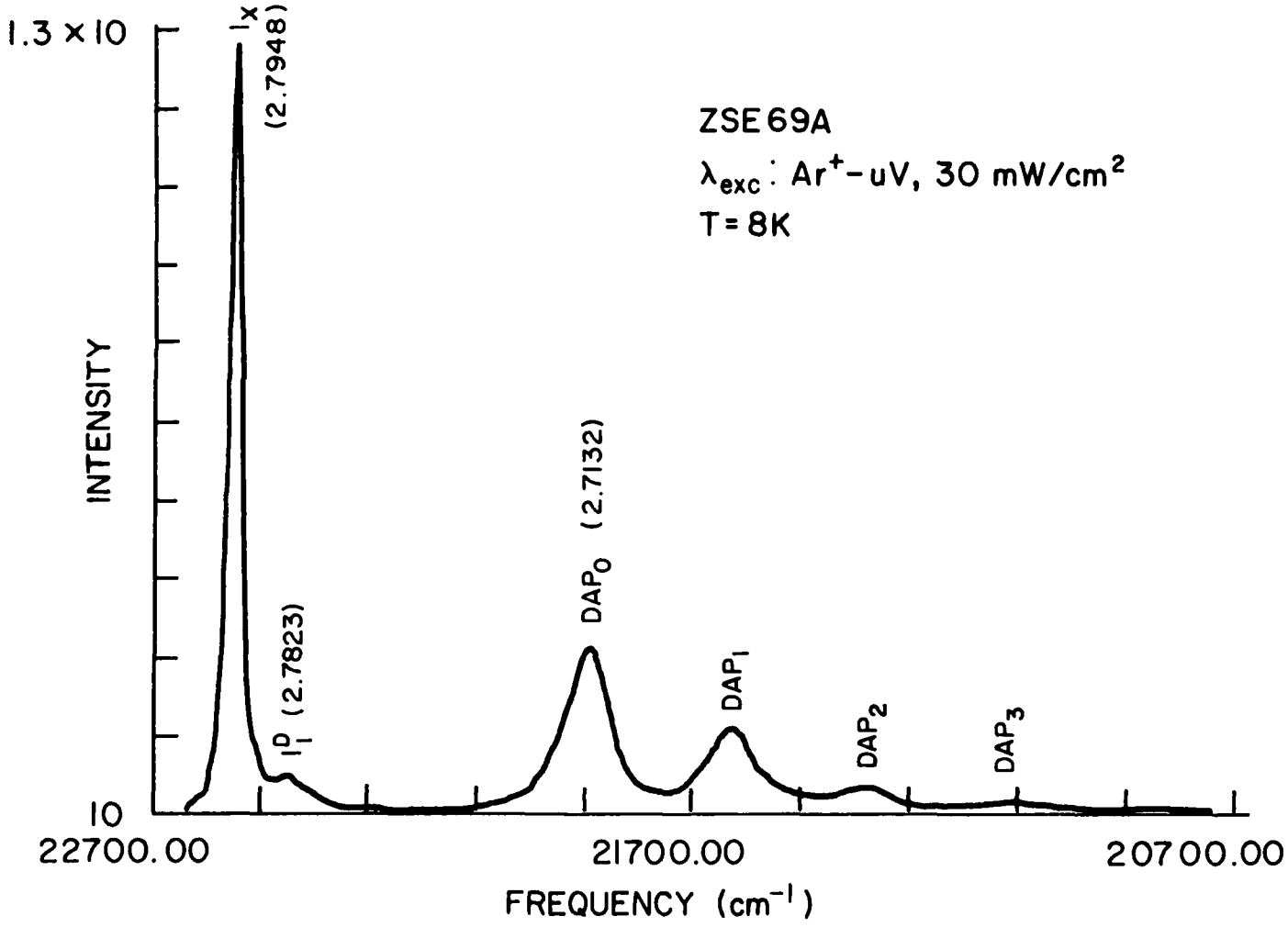

Figure 2-26. The 9K near-band-edge emission spectrum for Sample #ZSE69A. This spectrum is typical of those obtained for samples in this Na-doping series. The peak at 2.713 eV is the zero-phonon peak in a donor-acceptor (DA) pair series. LO-phonon overtones of this peak appear to lower energies, spaced by the 32 meV (256 cm^{-1}) LO-phonon energy.

Performing the standard calculation [8] with E_G = 2.82(18) eV at 4.2K, E_d = 27 meV, e^2/Kr = 10 - 15 meV, we find the acceptor binding energy from

$$h\nu = E_G - (E_D - E_A) + e^2/Kr$$

from which we calculate E_A = 92 - 97 meV. This value is considerably less than the published value of 126 meV [9] , but in agreement with the value reported by Yao [10]. Also in agreement with this latter report, we do not observe any evidence of acceptor-bound exciton (ABE) emission from this sample. For some of the samples grown later in the series, where considerably more Na was incorporated, there is a shoulder on the low energy side of the DBE peak near 2.784 - 2.787 eV; if this is an ABE peak it would correspond to acceptor binding energies 100 - 120 meV, in approximate agreement with the E_A derived above from the DAP zero-phonon line position. Several other features of the ZSE69A PL spectrum are worthy of note:

1. The intensity of I_x has not decreased significantly from what we had observed in the non-doping runs. Yao [10] saw I_x drop by about a factor of 20 by the time $I_{DAP} = 0.4\ I_x$.
2. The width of the DBE peak is about 3.5 meV--much larger than what we saw in previous (non-doping) runs. It appears that both I_x and I_2 have broadened to the point that we see a featureless, nearly-symmetric peak. This increased linewidth is consistent with the larger carrier concentrations and lower mobilities measured for these films.
3. There is a sizable I_1^{Deep} peak at 2.7823 eV (I_1^{Deep}/I_x = 0.5). Usually we see a peak I_1^{Deep} closer to 2.781 eV and I_1^{Deep}/I_x = 0.01. The I_1^{Deep} peak in ZSE69A is sufficiently large that it has precluded the possibility of performing selective excitation PL (SPL) measurements. The two-electron donor satellites (TEDS) should appear near 2.775 eV, but this falls on the low-energy tail of the strong I_1^{Deep} peak; it has proved impossible to discriminate the small signals from this strong background.
4. There has been no significant increase in the deep-level emission.

The PL measurements on the Na-doped samples are summarized in Table 2.3. Note that the DAP intensity increase monotonically as the Na_2Se oven temperature increases. As mentioned above in connection with ZSE69A, we do not see a decrease in the I_x intensity as the DAP intensity increases, as was reported by Yao [10], and as would be expected if the number of donors were to remain constant as the acceptor density increased. Instead, our PL data, as well as the electrical measurements on these samples, seem to indicate that additional donors are being incorporated along with the Na atoms. As discussed elsewhere in this report, we believe these additional donors come from contamination of the Na_2Se starting material.

2.2.1.3 ZnSe:Na Electrical Characterization

Six samples (ZSE68A - ZSE73A) were doped with Na using Na_2Se as a source of Na. The results of the Hall measurements for these samples are shown in Figures 2-27 and 2-28. The growth conditions were fixed at T_g = 350°C and BPR = 1/2:1 with the temperature of the Na_2Se cell variable for samples ZSE68A - ZSE70A. The growth temperature and temperature of the Na_2Se cell were fixed and the BPR variable for ZSE71A - ZSE73A.

Figure 2-29 shows the room temperature carrier concentration (n_{300}), the room temperature mobility (μ_{300}), and the peak mobility (μ_p) as a function of Na_2Se cell temperature (T_{Na}). For T_{Na} = 375°C the carrier concentration and mobilities appear unchanged from those of the undoped samples grown under these conditions. As T_{Na} is increased, the number of carriers increases and both μ_{300} and μ_p decrease. Shallow donors are introduced with increasing concentration as the Na_2Se oven temperature is increased. At this time the origin of the donors is unclear; impurities in the Na_2Se, modification of growth due to the presence of Na_2Se, or interstitial Na may each provide shallow levels.

In Figure 2-30 are plotted n_{300}, μ_{300}, and μ_p for ZSE71A - ZSE73A. This figure shows that acceptor incorporation may depend strongly upon the sample growth conditions. If it is assumed that the differences in mobility are due to ionized impurity scattering, then the room temperature and peak mobilities of ZSE71A and ZSE73A imply that the concentration of ionized impurities in ZSE73A is greater than in ZSE71A. If the room temperature carrier concentrations are compared, then the difference between the donor and acceptor concentration is greater in ZSE71A than in ZSE73A.

TABLE 2-3. Photoluminescence Data for samples in the Na-doping series

				I_x			I_1			DAP		DL
Sample #	T_G(°C)	BPR	T_{Na_2S}(°C)	E(eV)	Intensity	Δ E(meV)	E(eV)	Intensity	E(eV)	Intensity	E(eV)	Intensity
ZSE68A	350	1/2:1	375	2.7952	$9.4x10^4$	1.7			2.7125	$5.6x10^1$	2.10	$2.2x10^1$
ZSE69A	350	1/2:1	450	2.7948	$1.1x10^5$	3.5			2.7132	$2.2x10^4$	2.06	$1.1x10^2$
ZSE70A	350	1/2:1	500	2.7941	$1.3x10^5$	4.13			2.7190	$1.6x10^4$	2.03	$3.6x10^2$
ZSE71A	270	1/2:1	450	2.7951	$8.1x10^3$	5.0			2.7163	$5.3x10^4$	2.10	$3.2x10^1$
ZSE72A	350	1:1	450	2.7942	$1.0x10^5$	2.5			2.7111	$6.0x10^4$	2.03	$7.8x10^1$
ZSE73A	260	1:1	450	2.7961	$7.4x10^3$	5.4	2.7837	$7.52x10^2$	2.715	$1.5x10^2$	2.06	$9.6x10^1$

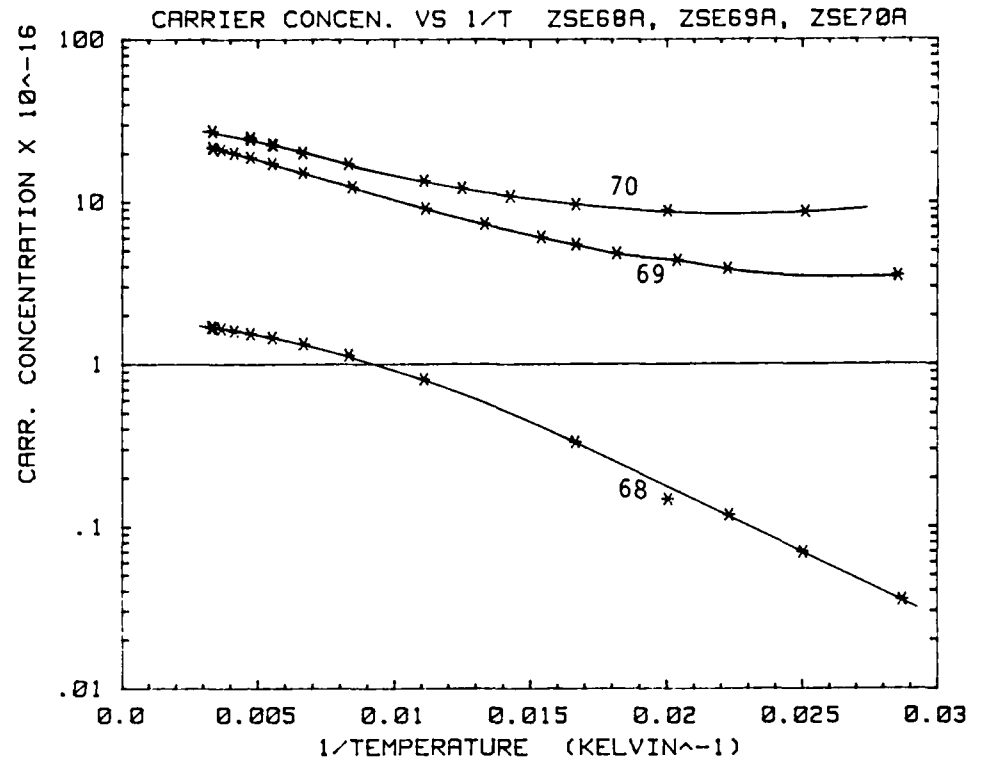

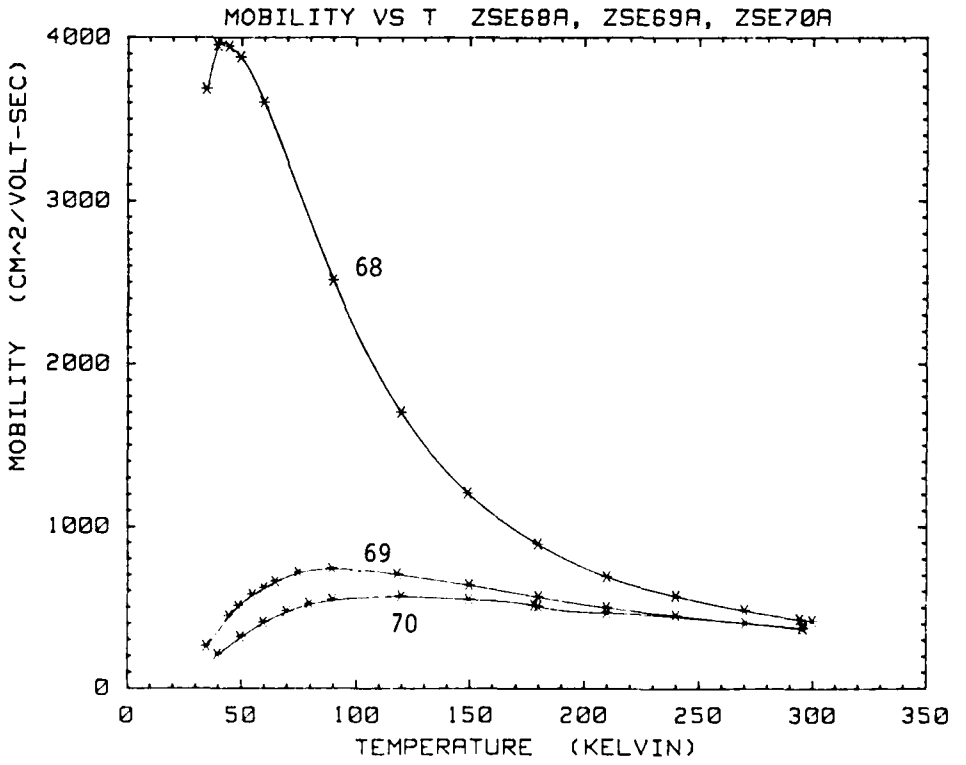

Figure 2-27. Electron concentrations and mobilities for Na-doped samples ZSE68-75. All samples were grown with T_g = 350°C, BPR = 1/2:1, and variable Na_2Se oven temperature. (See Table 2.1.)

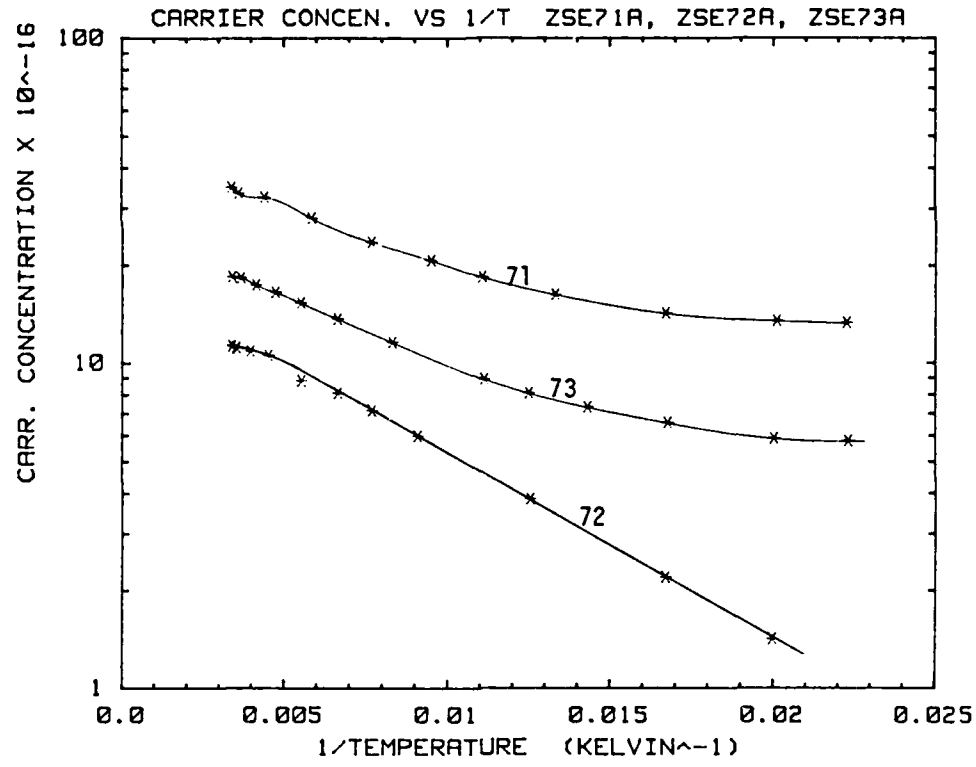

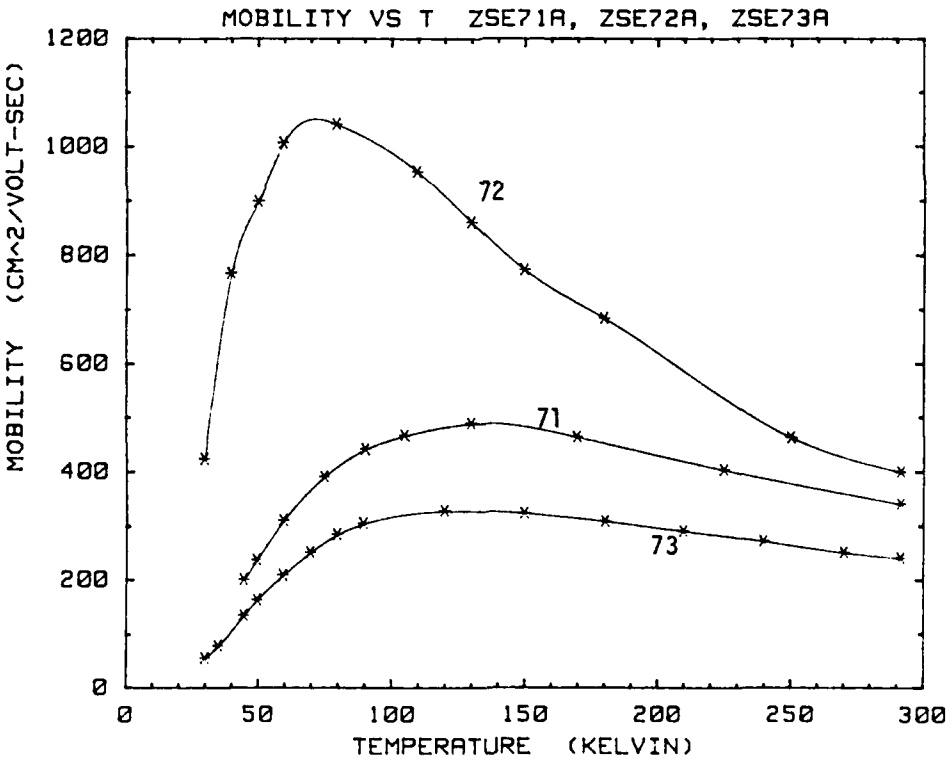

Figure 2-28. Electron concentrations and mobilities for Na-doped samples ZSE71-73. All samples were grown at a Na_2Se temperature of 450°C, but with differing T_g and BPR (See Table 2.1.)

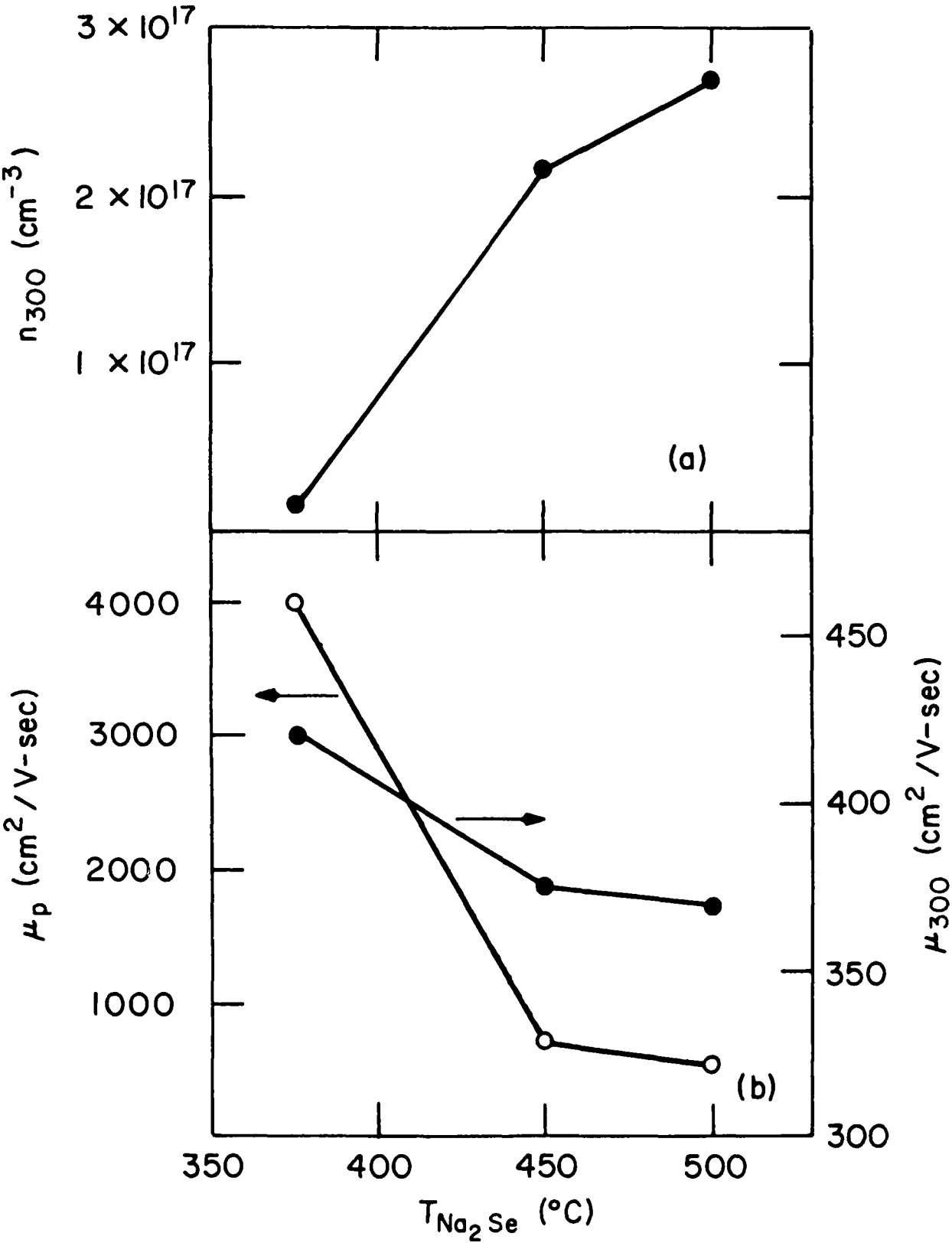

Figure 2-29. Room temperature electron concentrations (a), and peak and room temperature mobilities (b), for Na-doped sample ZSE68-70. Samples were grown at the same T_g and BPR, but with different Na_2Se oven temperatures. (See Table 2.1.)

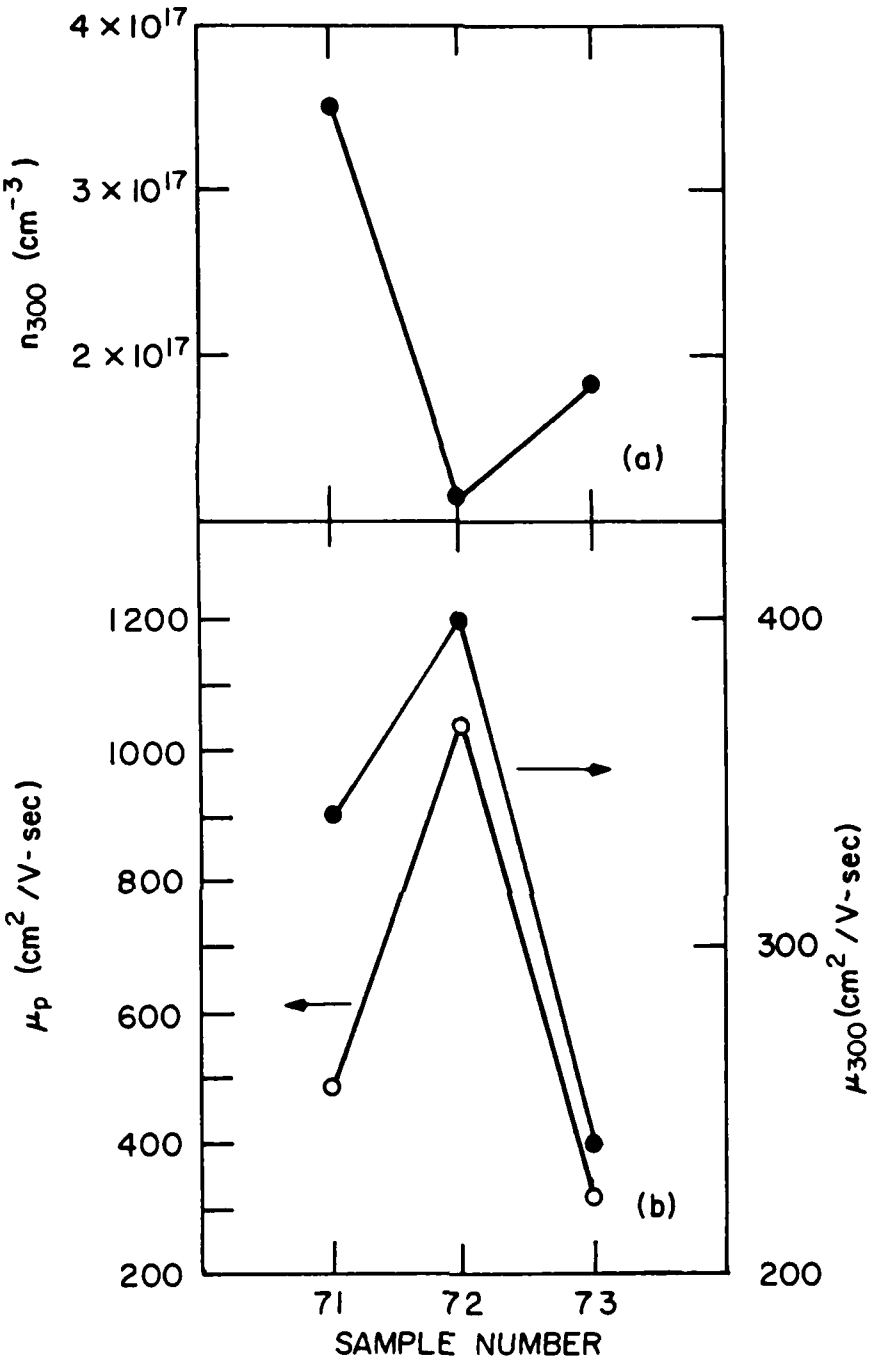

Figure 2-30. Room temperature electron concentrations (a), and peak and room temperature mobilities (b), for Na-doped samples ZSE 71-73. Samples were grown at the same Na_2Se oven temperature, but different T_g and BPR. (see Table 2.1.)

That is:

$$N_D + N_A \text{ (ZSE73A)} > N_D + N_A \text{ (ZSE71A)}$$
$$N_D - N_A \text{ (ZSE73A)} < N_D - N_A \text{ (ZSE71A)}.$$

From these inequalities it can be deduced that N_A (ZSE73A) > N_A (ZSE71A).

This result is consistent with the SIMS results reported elsewhere and reflects the importance of growth conditions in acceptor incorporation.

2.2.2 N_2-Doped ZnSe on (100) GaAs

Nitrogen doping was performed by using a high-precision leak valve to bleed N_2 gas into the growth chamber, allowing the establishment of prescribed N_2 pressures in the MBE chamber during growth.

2.2.2.1 ZnSe:N Growth Procedures

Several growth runs were made using an N_2 pressure in the chamber of 10^{-4} mbar, with a Zn to Se beam pressure ratio of 10:1 and a substrate temperature of 330°C. In addition, layers were grown using the above growth conditions without the introduction of N_2 in the growth chamber for comparison purposes. In both cases the layers were grown on sputtered and annealed GaAs substrates to thickness around 0.7 μm.

The RHEED patterns observed from the sputtered and annealed (100) GaAs substrates were indicative of (4 x 1) reconstructed surfaces. Figure 2-31 (a) shows the pattern recorded in the [1$\bar{1}$0] azimuth. The RHEED pattern recorded in this azimuth from an N_2-doped ZnSe layer following the deposition of around 1,000 Å of material is shown in Figure 2-31 (b), which is indicative of a smooth well-ordered surface. In fact, no deterioration of the RHEED pattern was observed for N_2-doped layers relative to unintentionally-doped layers.

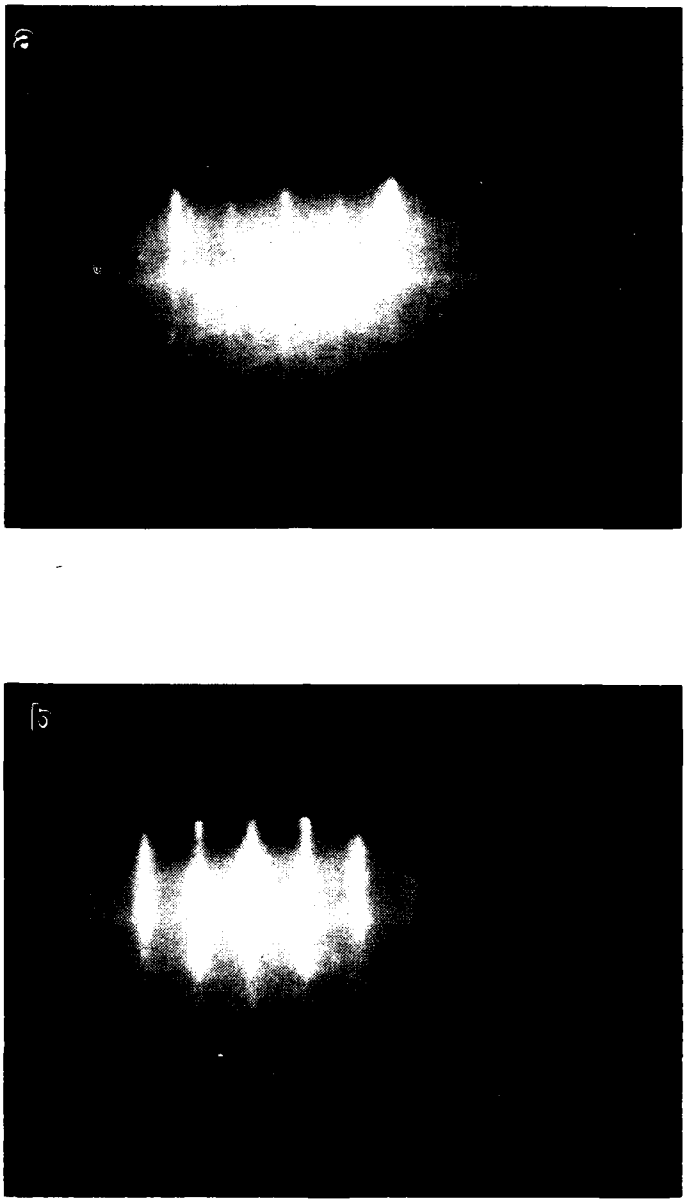

Figure 2-31. RHEED patterns recorded from (a) sputtered and annealed (100) GaAs and (b) N_2-doped ZnSe following 1,000 Å deposition (N_2 pressure = 10^{-4} mbar).

2.2.2.2 ZnSe:N Photoluminescence

The 4.2K photoluminescence spectra recorded from unintentionally-doped and N_2-doped layers are compared and contrasted in Figures 2-32 (a) and (b) and Figures 2-33 (a) and (b).

Figures 2-31 (a) and (b) illustrate the excitonic spectra recorded from unintentionally-doped and N_2-doped layers, respectively, both having a thickness around 0.7 μm. As can be seen from the figures, polariton emission dominates the spectrum recorded from unintentionally-doped layers, whereas an acceptor-bound exciton (I_1^N) at an energy of 2.793 eV due to nitrogen incorporation dominates the spectrum from N_2-doped material. Also, as can be seen from the figure, the ratio between the acceptor-bound and donor-bound (2.796 eV) exciton emission peaks is large. Figures 2-33 (a) and (b) show spectra recorded from unintentionally-doped and N_2-doped ZnSe layers, respectively, which include the D-A pair transition range. As can be seen from Figure 2-33 (a), D-A emission is essentially absent from the spectrum recorded from unintentionally-doped material, however, D-A emission in the form of a no-phonon peak (Q_o^N) together with its phonon replicas are clearly resolved in the spectrum of Figure 2-33 (b), recorded from N_2-doped material. An interesting point to note regarding the N_2-doped spectrum of Figure 2-33 (b) is that the intensity of the acceptor-bound exciton (I_1^N) is larger than that of the D-A emission.

2.2.2.3 ZnSe:N Electrical Characterization

Electrical measurements on nitrogen-doped ZnSe samples have proven to be very difficult due to the high resistivity of these samples. However, preliminary measurements have been made on one particularly interesting ZnSe:N sample, ZS195.

The PL spectra obtained from this sample were dominated by emission from the recombination of excitons bound to neutral acceptors, hinting that the material could be p-type. Although this sample was found to be too resistive for Hall measurements, the carrier type could be determined from contact studies. Both gold and indium contacts were deposited on a piece of ZS195. The results of the contact studies are shown in Figure 2-34.

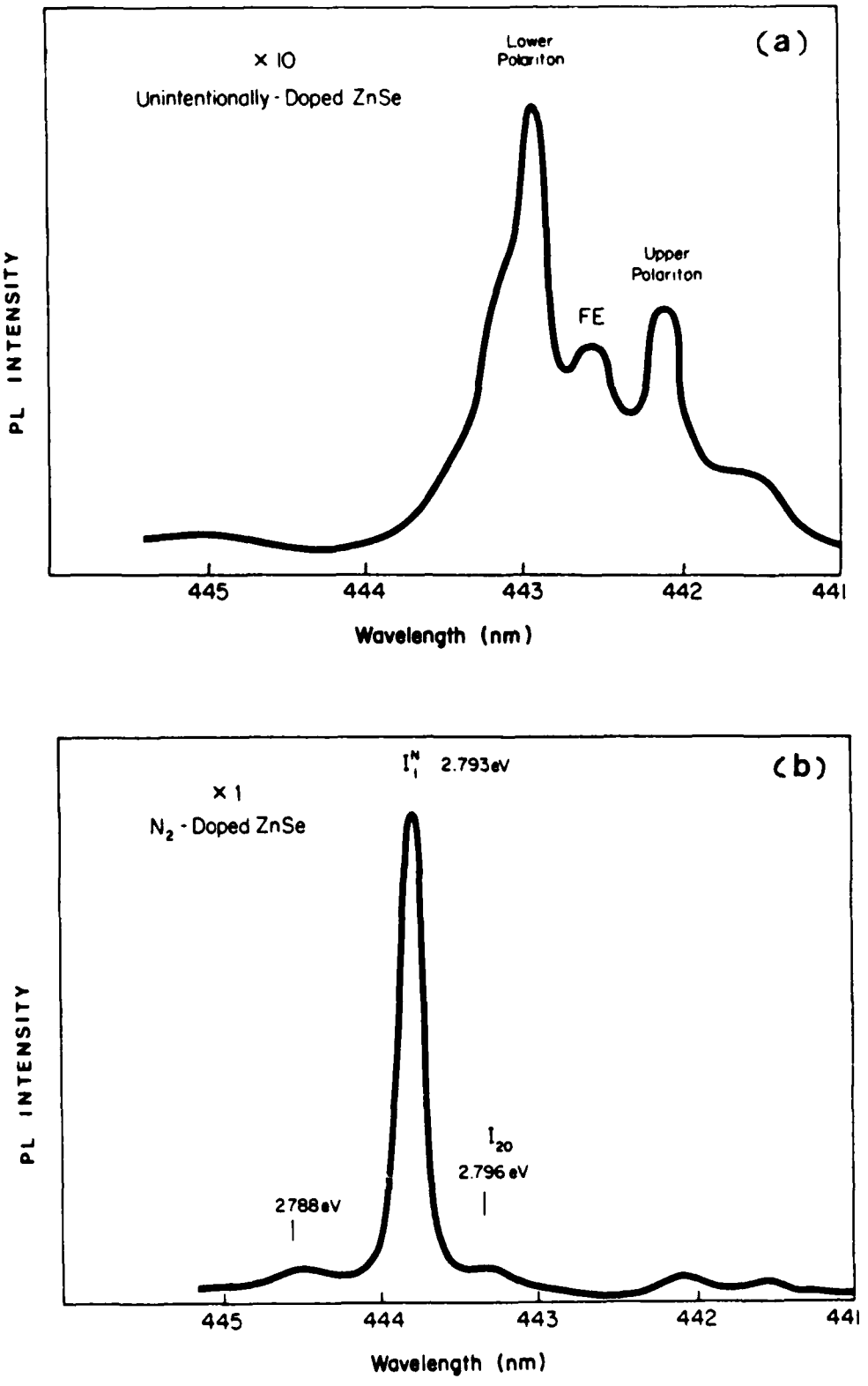

Figure 2-32. 4.2K PL excitonic spectra recorded from (a) unintentionally-doped ZnSe and (b) N_2-doped ZnSe. Both layers were grown using a 10:1 Zn to Se beam pressure ratio at 330°C to a thickness of 0.7 μm.

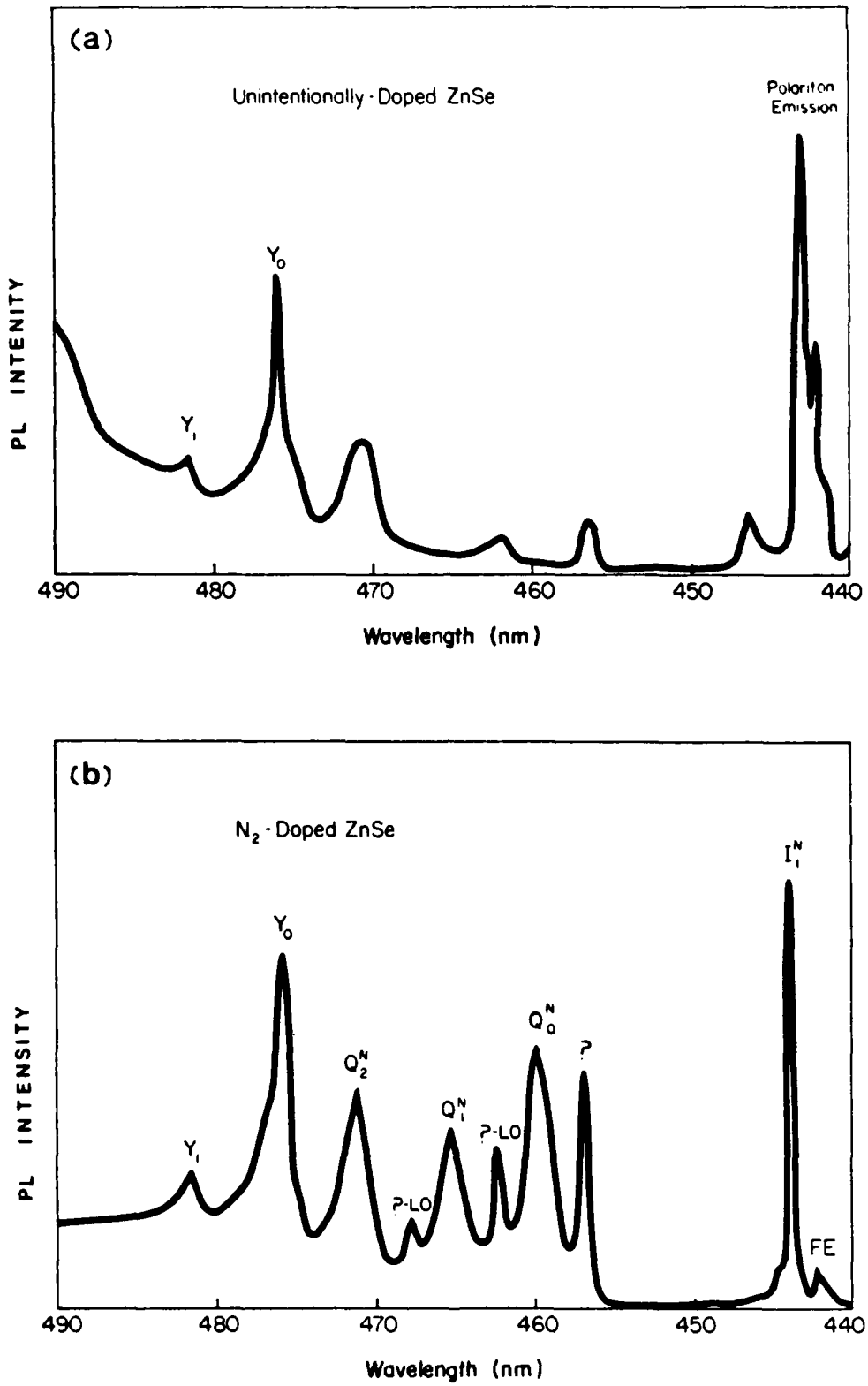

Figure 2-33. 4.2K PL spectra recorded from (a) unintentionally-doped ZnSe and (b) N_2-doped ZnSe. Both layers were grown using a 10:1 Zn to Se beam pressure ratio at 330°C to a thickness of 0.7 μm.

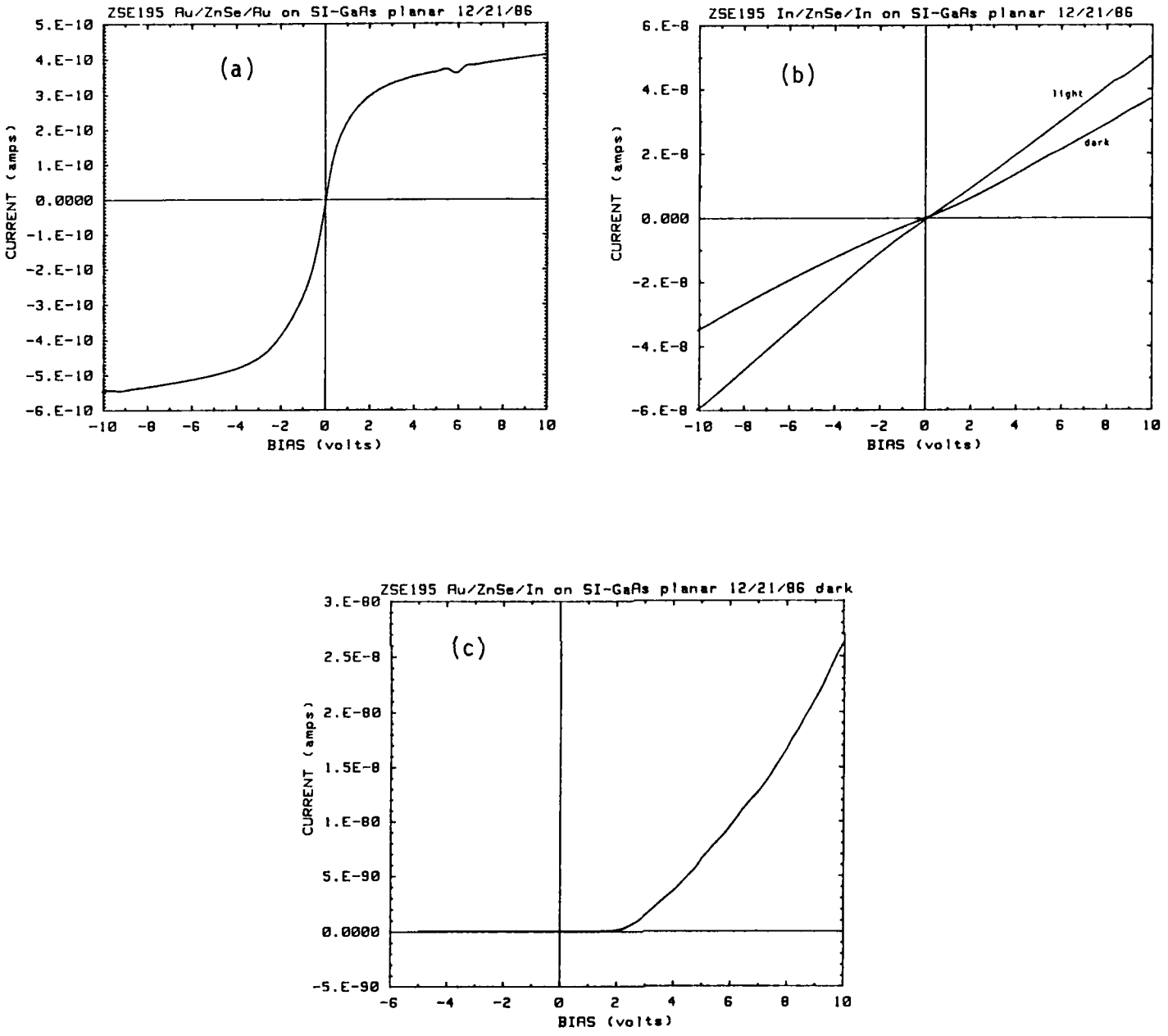

Figure 2-34. Results of current-voltage (coplanar) contact studies on N-doped ZnSe sample ZSE195.
a) Characteristics for back-to-back Au/ZnSe contacts showing Schottky behaviors.
b) Characteristics for back-to-back In/ZnSe contacts.
c) Characteristics for a Au/ZnSe/In coplanar structure.

The I-V characteristics obtained from Au/ZnSe/Au (Figure 2-34 (a)] are similar to those expected for back-to-back diodes. The I-V curves obtained from In/ZnSe/In [Figure 2-34 (b))] on the other hand, are linear indicating the formation of ohmic contacts. Indium is known to form ohmic contacts to n-type ZnSe whereas Au may be used for ohmic contacts on p-type ZnSe. Sample ZS195, therefore, is high resistivity n-type material, in spite of the PL results.

2.3 Project 2, Task 1: Device Research - Photopumping, e-Beam Pumping and Cavity Formation

2.3.1 e-Beam Pumping Measurement

Electron-beam pumping efforts continued this quarter; both our own MBE-grown samples and Northwestern University OMVPE-grown ZnSe samples were used in cavity fabrication.

We have extended our measurements on a thick film (ZSE48A, 4.3 μm) to study some of the dynamic aspects of the lasing process and to attempt to identify the lasing mechanisms prevailing in different temperature and excitation density regimes. Figure 2-35 shows the spectrum (T = 16K, V_{acc} = 35 kV) of the emitted light from ZSE48A11 at a pumping level above the lasing threshold (J_{th} = 2.4 A/cm^2) for this sample. This spectrum was obtained using an 1800 lines/mm, rather than our normal 600/mm, grating to disperse the light; the increased dispersion serves to demonstrate the extremely small width of the lasing lines (< 1 Å in some cases).

In order to measure the gain profile of the ZnSe films under electron beam excitation, we have employed a modification of a technique used in optical pumping [11]. The spectrum is measured as the beam is moved off the edge of the sample. At any given wavelength, the intensity can then be obtained as a function of the length, d, of the sample through which the light traverses:

$$I(d) = I_o \ (e^{g(\lambda)d} - 1).$$

By fitting the data at each wavelength to an exponential, one can obtain an estimate of the gain, $g(\lambda)$, at that wavelength, temperature and excitation density.

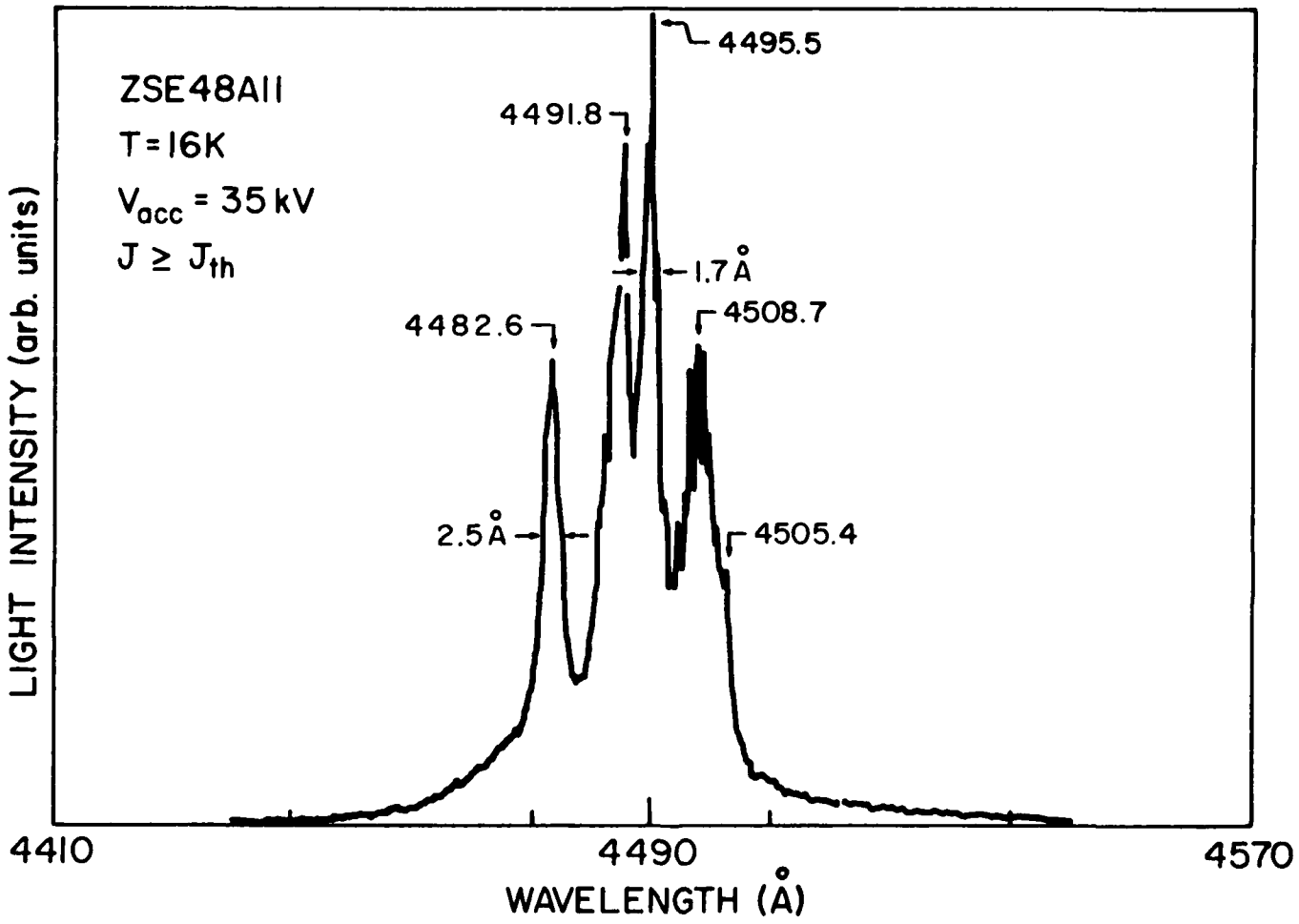

Figure 2-35. High resolution scan of the spectral output for sample ZSE48A11 under electron beam excitation at a current density above threshold. T = 16 K. V_{acc} = 35 kV.

Our preliminary measurements of the gain profiles obtained for ZSE48A at 16, 160 and 300 K at current densities just below threshold are shown in Figure 2-36. The gain curves have been normalized to the same peak value in order to emphasize the spectral features of the curves. We are beginning calculations of gain profiles expected for different lasing mechanisms in order to identify which mechanism are applicable in our case.

We have also made more detailed measurements of the time dependence of the lasing output using the higher time resolution available with the boxcar integrator. With the boxcar, we can work with a 1 - 3 ns gate, whereas the optical multichannel analyzer gate can be no shorter than 20 ns. Figure 2-37 shows the time evolution of the light output pulse (ZSE48A11, 16K, 35 kV, 4480 Å) at pumping current densities $J << J_{th}$, $J < J_{th}$, $J > J_{th}$, $J >> J_{th}$, and $J >>> J_{th}$ for (a), (b), (c), (d), and (e) respectively. Note that at very low current densities [Figure 2-37 (a)], the light output follows the electron beam profile quite well; the pulse is approximately square and has a flat top. As the current increases [Figure 2-37 (b)], the light pulse becomes asymmetric, increasing with increasing time, peaking where the initial lasing pulse is about to emerge [see Figure 2-37 (c)]. Initially, the lasing occurs in a single peak, turning on at about 40 ns after the start of the electron beam pulse, rising to a maximum, and then shutting off at about 60 ns after the start of the excitation. As the pumping current density is made still larger [Figure 2-37 (d)], a new, 'early' peak emerges at 20 ns into the excitation; this emission is quenched and then succeeded by the 'later' pulse of similar amplitude. At still higher current densities [Figure 2-37 (e)], the 'early' peak dominates the light output. It would appear that, near threshold, some 'slow' mechanism is active in producing the late pulse about 50 ns into the excitation, but as J increases we arrive at a sufficiently high density to activate a 'fast' mechanism which then gives rise to the 'early' pulse. The quenching of the two modes could be produced by heating of the active region, which moves the material into a region where the operative mechanism no longer has sufficient gain. Alternatively, the quenching could just be the result of the population inversion decreasing as the gain overshoots the cavity losses, causing the lasing to 'spike' as is the case in some other laser systems [12]. Figure 2-38 shows the spectra recorded using the boxcar integrator with a 3 ns gate centered on several of the features observed in Figure 2-37.

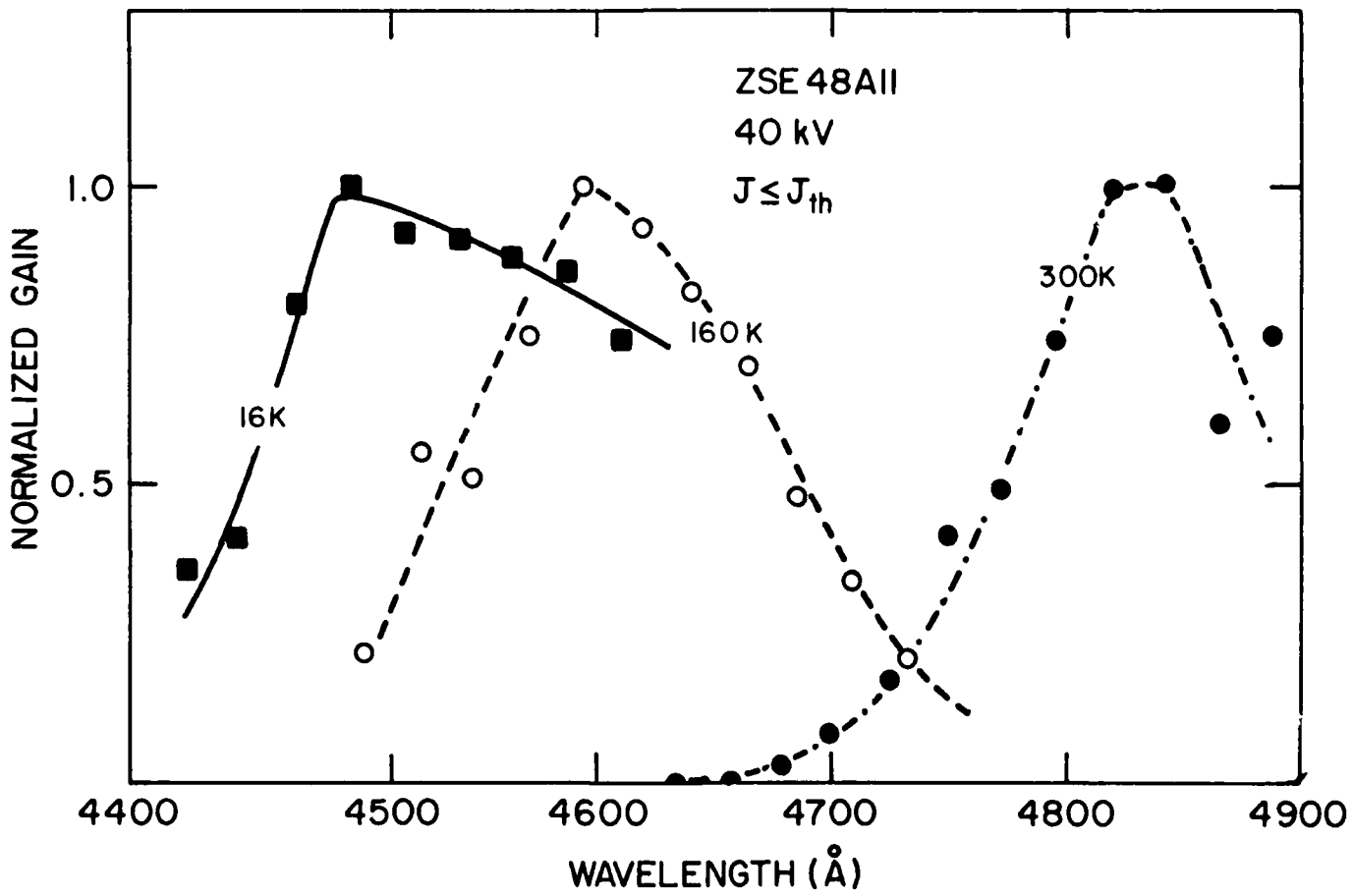

Figure 2-36. Measured normalized gain curves for electron-beam-pumped ZnSe sample #ZSE48A11 at a current density just below threshold at temperatures of 16, 160 and 300K.

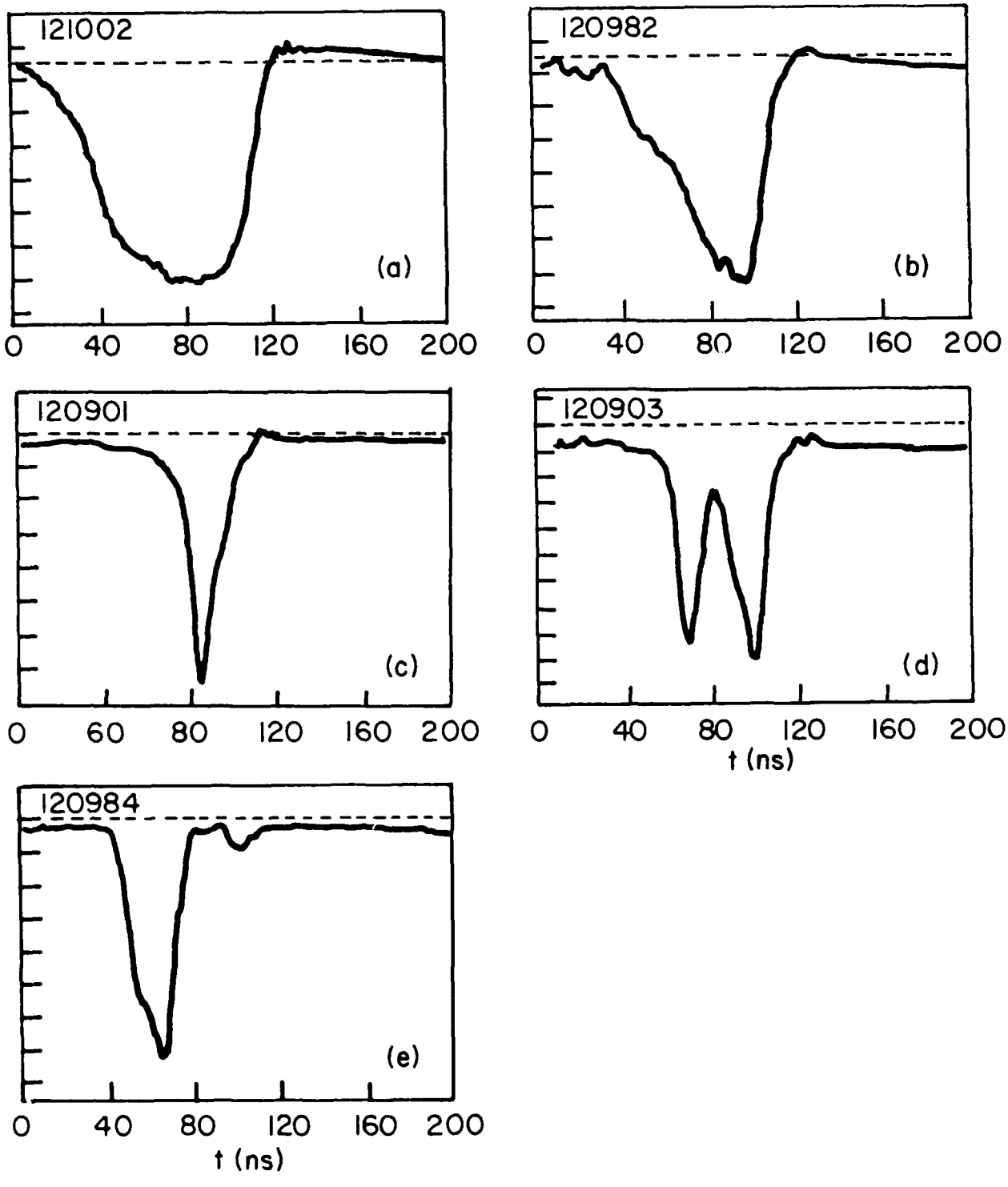

Figure 2-37. Evolution of the light output pulse from electron-beam-pumped MBE-ZnSe with increasing beam current density. (a) and (b) are below threshold, while (c) - (e) are above threshold.

Figure 2-38 (a) shows the result of placing the gate on the single narrow spike when $J > J_{th}$ [Figure 2-36 (c)], while Figure 2-38 (b) and (c) show the different spectra which result when the gate is on the 'early' and 'late' pulses in the $J >> J_{th}$ case [Figure 2-37 (d)]. Clearly, the spectrum shifts to longer wavelengths for the 'late' pulse. Experimental and theoretical work is underway in an attempt to understand this behavior.

We have also electron-beam pumped two thick ($t = 4 - 6$ μm) samples of OMVPE-grown ZnSe/(100) GaAs provided to us by Prof. B. Wessels of Northwestern University. One of these samples (Y194) was made to lase, but only under the most extreme excitation conditions: 16K, 40 kV, $J_{th} = 20$ A/cm^2. The other sample (Y193a) could not be brought to lasing under any conditions. (It should be noted, however, that the electron beam was observed to defocus at the extremely high currents employed here; it may be that these films were extremely resistive, so that the film charged up under electron beam excitation, causing the observed defocussing.) While both of these films exhibited dominant NBE emission in their PL spectra, the overall luminescence emission efficiency of these OMVPE films is at least an order of magnitude smaller than that of our MBE films. This helps to affirm our belief in a correlation between high NBE emission intensity and low lasing thresholds. Some additional OMVPE films will be examined during the next quarter.

2.4 Project 2, Task 2: Contact Studies

2.4.1 Ohmic Contacts

The ohmic contact studies were initiated for the purpose of making ohmic contacts to ZnSe grown on p-GaAs, thus eliminating the interface problems experienced with metal Schottky barriers on ZnSe. We have done resistivity measurements on ZnSe (on SI GaAs substrate) using planar Al/In contacts annealed at 300°C for 10 minutes. Resistivity, ρ, as a function of temperature is shown in Figure 2-39. A minimum in ρ is observed at 130°K consistent with Hall measurements; resistivity measured in the coplanar configuration is approximately two times higher than that measured by Hall measurements. In several samples we have also observed resistivity values in the coplanar configuration lower than the Hall measurements by a factor of two. This is probably due to contact resistance effects. We have not initiated any contact resistance studies as yet.

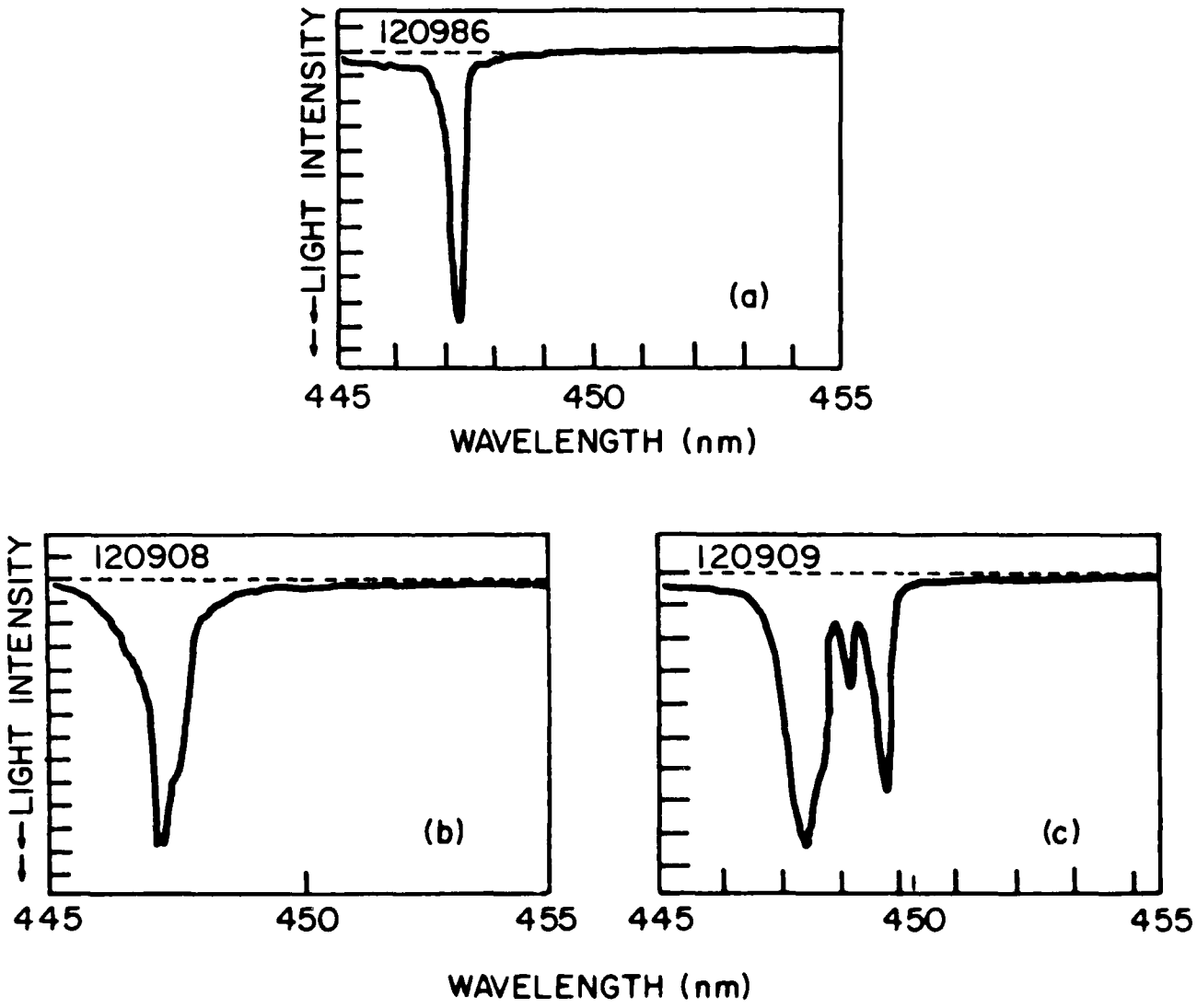

Figure 2-38. Evolution of the spectral output from electron beam-pumped MBE-ZnSe with increasing beam current density. All three scans were taken at current densities above threshold; (a) - (c) here correspond to (c) - (e) in the previous figure.

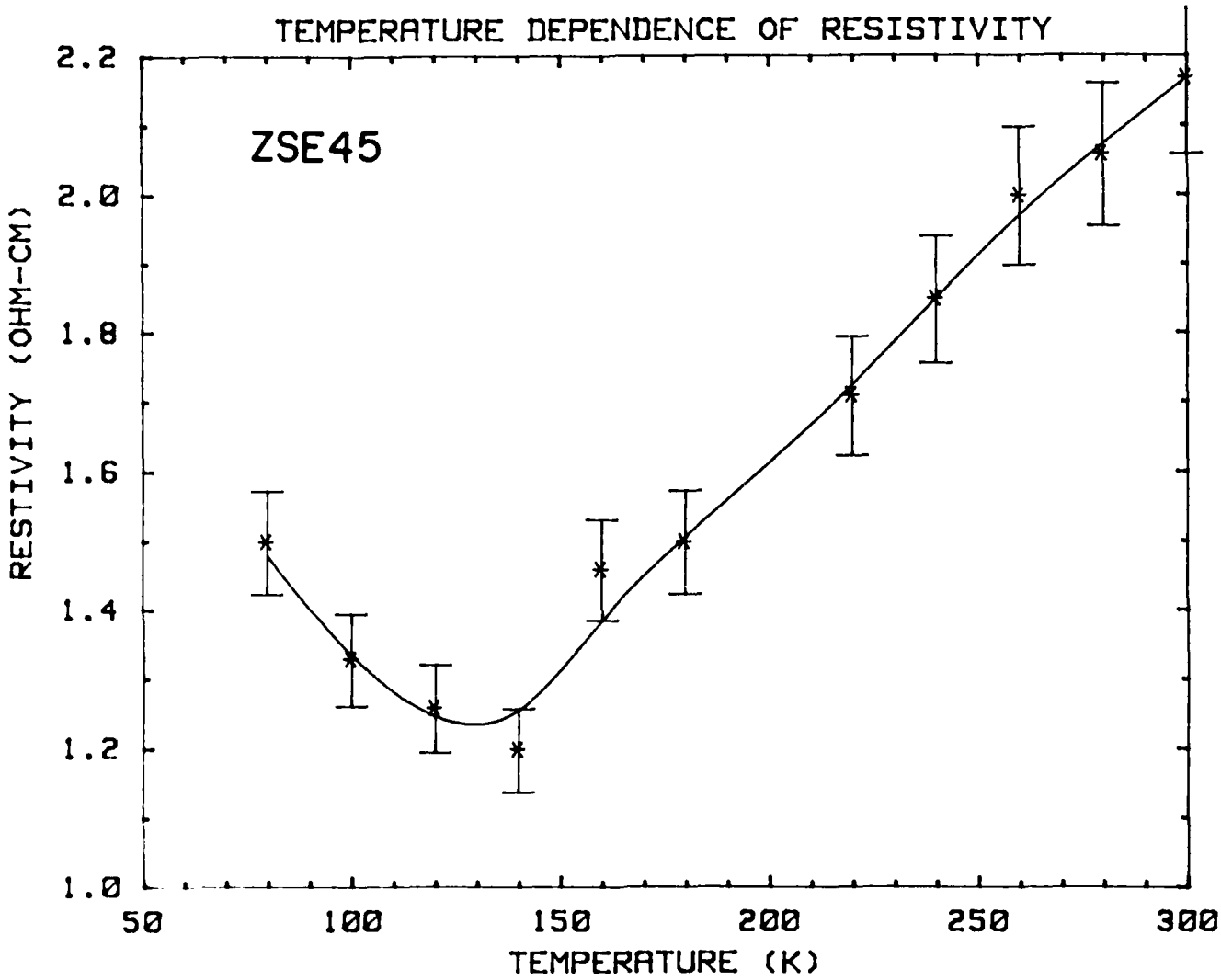

Figure 2-39. Temperature dependence of resistivity for unintentionally-doped ZnSe.

In order to understand the ohmic contact formation behavior of In on ZnSe, In contacts on ZnSe were studied by SEM before and after annealing, and In/Al contacts were studied after annealing (at 300°C). The results are summarized below:

i) Thin In films were discontinuous before and after annealing.

ii) Thick In films (> 2.0 kÅ) were continuous before annealing, but formed separated islands after annealing. These separated islands are responsible for poor ohmic contacts with thicker film.

iii) Thicker In with Al overlayers gave more reproducible ohmic contact characteristics.

iv) Several In/Al contacts showed nodular features (probably In) beneath the Al overlayer. This indicates the strong island formulation tendency of indium due to its high surface tension. However, the aluminum overlayer prevents strong segregation of the In, and forms a continuous metal layer in the contact region.

v) Aluminum films < 2000 Å show cracks after annealing, probably again due to the high surface tension of In.

3.0 REFERENCES

1. A.Y. Cho, Thin Solid Films, 100, 291 (1983).

2. J.L. Merz, H. Kukimoto, K. Nassau, and J.W. Shiever, Phys. Rev. B6, 545 (1972).

3. Peter Y. Yu and J.E. Smith, Jr., Phys. Rev. Letters 37, 622 (1976).

4. Quarterly Technical Progress Report No. 2, Blue-Green Laser Diode Research Program, prepared under Contract Number N00014-85-C-0552 with DARPA, October 1986.

5. A.K. Sood, J. Menendez, M. Cardona and K. Ploog, Phys. Rev. Letters 54, 2115 (1985).

6. C.T. Shah and V.G.K. Reddi, IEEE Trans. Electron Devices, ED-11, 345 (1964).

7. T.O. Yep and R.J. Archer, Scientific Report, AFCRL-67-0530 (1967).

8. T. Yao and Y. Okada, Jpn. J. Appl. Phys. 25, 821 (1986).

9. R.N. Bhargava, J. Cryst. Growth 59, 15 (1982).

10. T. Yao and T. Taguchi, Proc. 13th Intl. Conf. on Defects in Semiconductors (Inst. Phys. Conf. Series, 1983), p. 1221.

11. K.L. Shaklee and R.F. Leheny, App. Phys. Letters 18, 475 (1971).

12. W. Demtroder in Laser Spectroscopy, Springer Series in Chem. Phys., Vol. 5 (Springer-Verlag, Berlin, 1981), p. 546.

END

3-87

DTIC